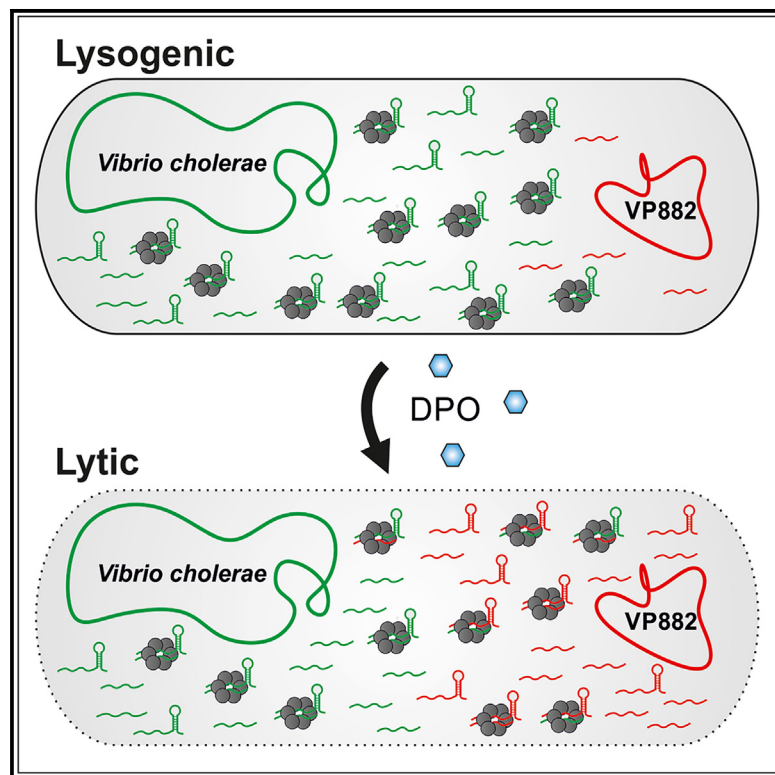


Small RNAs direct attack and defense mechanisms in a quorum sensing phage and its host

Graphical abstract



Authors

Marcel Sprenger, Malte Siemers,
Sebastian Krautwurst, Kai Papenfort

Correspondence

kai.papenfort@uni-jena.de

In brief

Activation of the lysogenic phage VP882 triggers intricate transcriptomic shifts in *V. cholerae*. Sprenger et al. reveal that phage activation promotes sRNA base pairing with host or phage transcripts via the RNA chaperone Hfq. Phage- and host-encoded sRNAs regulate gene expression at the post-transcriptional level to either enhance or inhibit phage replication.

Highlights

- Activation of phage VP882 results in complex transcriptional changes in *V. cholerae*
- The Hfq RNA chaperone supports interactions of host- and phage-encoded transcripts
- The phage-encoded VpdS sRNA facilitates phage replication
- Host-encoded sRNAs inhibit phage replication through base-pairing interactions



Article

Small RNAs direct attack and defense mechanisms in a quorum sensing phage and its host

Marcel Sprenger,¹ Malte Siemers,^{1,2} Sebastian Krautwurst,¹ and Kai Papenfort^{1,2,3,*}

¹Friedrich Schiller University, Institute of Microbiology, 07745 Jena, Germany

²Microverse Cluster, Friedrich Schiller University Jena, 07743 Jena, Germany

³Lead contact

*Correspondence: kai.papenfort@uni-jena.de

<https://doi.org/10.1016/j.chom.2024.03.010>

SUMMARY

Many, if not all, bacteria use quorum sensing (QS) to control collective behaviors, and more recently, QS has also been discovered in bacteriophages (phages). Phages can produce communication molecules of their own, or “listen in” on the host’s communication processes, to switch between lytic and lysogenic modes of infection. Here, we study the interaction of *Vibrio cholerae* with the lysogenic phage VP882, which is activated by the QS molecule DPO. We discover that induction of VP882 results in the binding of phage transcripts to the major RNA chaperone Hfq, which in turn outcompetes and downregulates host-encoded small RNAs (sRNAs). VP882 itself also encodes Hfq-binding sRNAs, and we demonstrate that one of these sRNAs, named VpdS, promotes phage replication by regulating host and phage mRNA levels. We further show that host-encoded sRNAs can antagonize phage replication by downregulating phage mRNA expression and thus might be part of the host’s phage defense arsenal.

INTRODUCTION

Bacteriophages, or short phages, are viruses that prey on bacteria and are considered the most abundant biological entities in the biosphere.¹ The interaction of phages with their hosts is highly diverse and likely one of the major drivers of bacterial evolution.² More recently, research on host-phage interactions has uncovered a plethora of bacterial defense strategies that frequently constitute ancient homologs of eukaryotic immune systems.^{3,4} Likewise, phages have developed sophisticated counter-defense strategies that target bacterial immunity, revealing an ongoing arms race between phages and their hosts.⁵

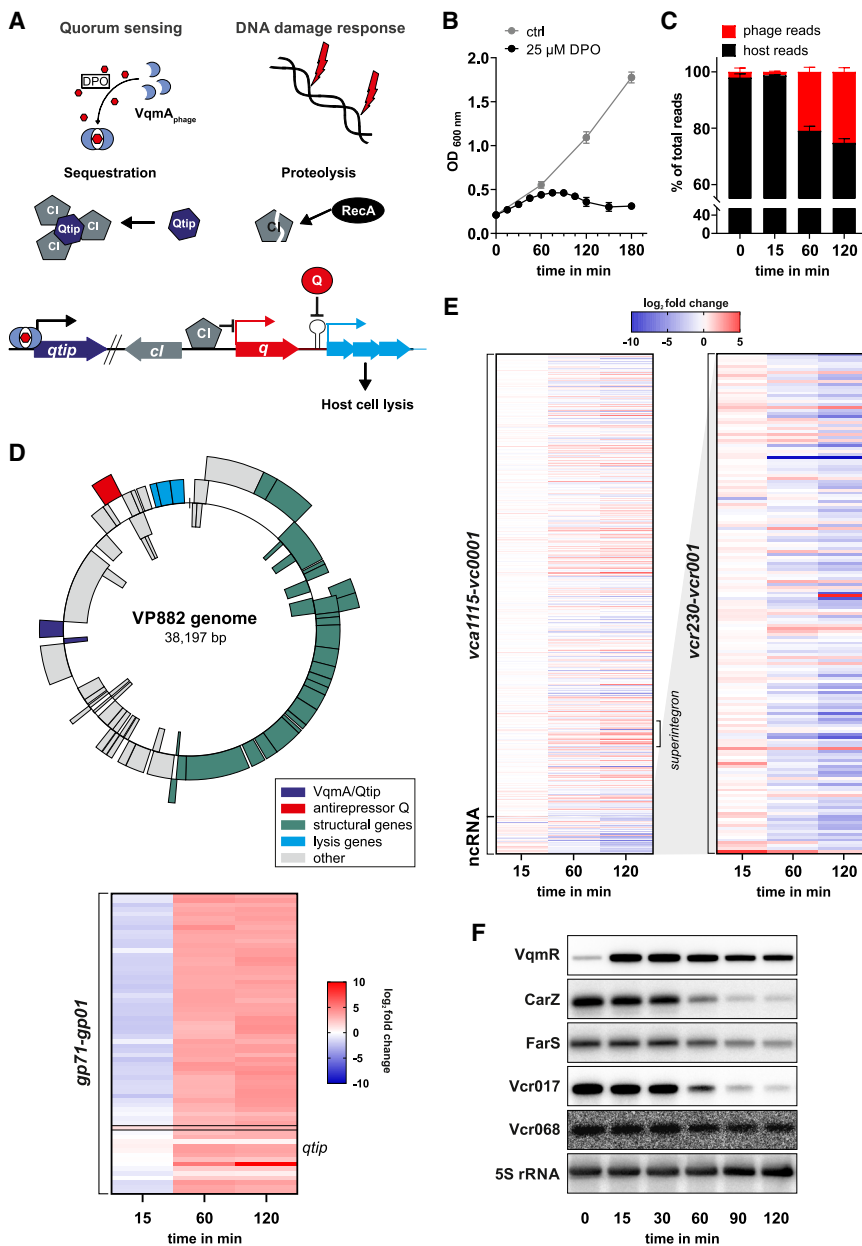
Viruses and phages have long been considered solitary entities. However, this view has now been challenged by the discovery of various phage-encoded quorum sensing (QS)-like communication systems.⁶ For example, phi3T, a lysogenic phage infecting *Bacillus subtilis*, employs a peptide-mediated communication strategy (called the arbitrium system) to measure phage concentration in the vicinal environment and to coordinate the switch between lytic and lysogenic lifestyles.⁷ Similarly, the lysogenic vibriophage VP882 harnesses a phage-encoded transcription factor that is homologous to the VqmA QS receptor protein of its host.^{8,9} Both proteins respond to the autoinducer molecule, 3,5-dimethylpyrazin-2-ol (DPO); however, only the phage-encoded VqmA protein activates the lytic program in VP882. Here, phage VqmA induces the production of a small protein, called Qtip, that sequesters the CI repressor protein of VP882 and thereby activates the phage lysis program⁸

(Figure 1A). Of note, analogous communication systems have now been discovered on hundreds of phage genomes, indicating that QS sensing phages are prevalent in nature.^{10–13}

While the above systems both use QS to “decide” between lytic and lysogenic modes of infection, they differ in how the QS signal is produced. Specifically, whereas the signalling peptides of the arbitrium system are encoded on the phage genome, DPO is produced by the host cell through the degradation of L-threonine via threonine dehydrogenase (Tdh).¹⁴ Binding of DPO to the host-encoded VqmA protein activates the transcription of the VqmR small RNA (sRNA), which inhibits biofilm formation and virulence gene regulation in *V. cholerae*.^{14–16}

VqmR belongs to the large class of Hfq-binding sRNAs that are prevalent in bacteria and that control gene expression by base-pairing with multiple target transcripts.¹⁷ Hfq was initially identified in *Escherichia coli* as a host factor facilitating the replication of the Qβ RNA phage¹⁸ and has now been studied in numerous other organisms as well. Mutation of the *hfq* gene is typically associated with pleiotropic phenotypes including reduced virulence in pathogenic bacteria.¹⁹ For example, lack of *hfq* impedes gut colonization by *V. cholerae* and prevents QS signaling, suggesting that Hfq-binding sRNAs could regulate both of these processes.^{20,21} Indeed, in addition to VqmR, *V. cholerae* encodes more than 80 Hfq-binding sRNAs²² that are involved in hundreds of RNA-RNA interactions.²³ Specifically, VqmR was shown to engage RNA duplex formation with multiple target transcripts, such as *vpsT*, encoding a major transcriptional activator of biofilm formation, and *aphA*, which is involved in various collective behaviors including pathogenicity.^{15,16}





with $25 \mu\text{M}$ DPO at $\text{OD}_{600} 0.2$ (pre). At indicated time points, RNA was collected and subjected to northern blotting using specific oligonucleotide probes. Probing for the ribosomal RNA 5S served as a loading control.

See also Figure S1.

Other Hfq-binding sRNAs with documented roles in virulence gene expression in *V. cholerae* are VcdRP,²⁴ VrrA,^{25,26} TarA,²⁷ and TarB.^{27,28} TarA and TarB are encoded on the *Vibrio* pathogenicity island (VPI), and the expression of both is controlled by the virulence-associated transcription factor, ToxT.^{27,29} VPI is a horizontally acquired genomic island in the genome of *V. cholerae* and key for host colonization and pathogenesis.³⁰ Interestingly, the VPI-encoded TarA sRNA has been reported to inhibit the expression of *ptsG*, which is encoded in the core genome of *V. cholerae*,²⁹ suggesting cross-regulation between core and accessory genomic elements by Hfq-binding sRNAs. In fact, similar observations have been made in other enteric patho-

gens^{31,32}; however, the role of RNA-RNA interactions during lytic activation of temperate phages is currently unknown.

To address this question, we recorded the transcriptomes of *V. cholerae* and VP882 following activation of the phage lysis program by DPO. We discovered hundreds of deregulated transcripts and mapped transcription initiation events in both genomes. Activation of VP882 resulted in the binding of phage-derived transcripts to Hfq, which in turn led to the downregulation of host-encoded Hfq-binding sRNAs. We discovered that the phage-encoded VP882 phage-derived sRNA (VpdS) sRNA is a major interaction partner of Hfq following phage induction and show that it is produced from the 3' untranslated region

Figure 1. The host and phage transcriptional response during DPO-induced VP882 activation

(A) Lysogenic VP882 can activate its lysis program through the DNA damage pathway or DPO-mediated activation of Qtip by sensing the cell density of the host population. This pathway is dependent on the DPO-binding transcription factor VqmA_{phage}, which activates the expression of *qtip*. The small protein Qtip (dark blue) sequesters the Cl protein (left), whereas DNA damage results in RecA-mediated proteolysis of the Cl repressor (right). Independent of the input signal, reduced Cl availability results in the derepression of the phage gene *q* and subsequent transcriptional activation of the lysis operon (light blue).

(B) Growth kinetics of *V. cholerae* lysogenized with VP882. Cells were grown to $\text{OD}_{600} 0.4$, back diluted 1:10 in M9 medium plus 0.035% arabinose (pre, 0 min), and treated at $\text{OD}_{600} 0.2$ with H_2O (gray) or $25 \mu\text{M}$ DPO (black). Dots show the mean of independent biological replicates \pm SD, $n = 3$.

(C) The percentage of total reads mapped to the bacterial and phage genome during the activation of VP882. Bars show the mean of independent biological replicates \pm SD, $n = 3$.

(D and E) Heatmaps of genome-wide transcriptional changes of VP882 (D) and host genes (E) in response to phage activation after treatment with $25 \mu\text{M}$ DPO. (D) Upper panel: genome map highlighting the structural genes, the host cell lysis genes, and the VqmA_{phage}-Qtip regulatory module of phage VP882. Lower panel: transcriptional changes of VP882 activation. Expression of *qtip*, as a primary target gene of the transcription factor VqmA_{phage}, is highlighted. (E) On the host site, VP882 activation affected the expression of ncRNA (tRNA, rRNA, and sRNA) and the super-integron. (F) Heatmap of transcriptional changes of host sRNA during phage activation. Fold changes of the normalized expression were calculated relative to the normalized expression value before treatment (pre, 0 min). Host genes were denoted by their location on the genome (chromosome 1: vc0001-vc2775, chromosome 2: vca0001-vca1115, and ncRNAs: vcr001-vcr230).

(F) Expression of various host sRNAs during VP882 activation. *V. cholerae* Δtda cells lysogenized with VP882 were grown to $\text{OD}_{600} 0.4$, back diluted 1:10 in M9 medium plus 0.035% arabinose, and treated with $25 \mu\text{M}$ DPO at $\text{OD}_{600} 0.2$ (pre). At indicated time points, RNA was collected and subjected to northern blotting using specific oligonucleotide probes. Probing for the ribosomal RNA 5S served as a loading control.

(UTR) of the *gp29* gene via RNase E-mediated processing. Global identification of Hfq-mediated RNA-RNA interactions following VP882 activation revealed pervasive RNA duplex formation between phage and host transcripts, including base-pairing of VpdS with multiple host and phage transcripts. Accordingly, mutation of *vpdS* delays VP882 replication and phage-mediated cell lysis. On the contrary, we discovered that the host-encoded TarB sRNA inhibits the expression of the phage lysis genes and thus impairs phage replication. Taken together, our findings provide evidence that Hfq-mediated base-pairing between host and phage transcripts is ubiquitous during VP882 activation and that both the phage and the host harness Hfq-binding sRNAs to manipulate phage replication to their own benefit.

RESULTS

Transcriptomic analysis of VP882 induction

Temperate phages co-exist with their bacterial hosts either as part of the host's genome or as phage-plasmids.³³ Induction of phage replication and the assembly of phage particles is well known to be triggered by DNA damage; however, several recent studies revealed that QS molecules also participate in this process.³⁴ QS-mediated phage activation was initially described for vibriophage VP882, which replicates in and lyses *V. cholerae* C6706 in response to DPO (Figure 1A). Of note, VP882 does not re-infect the *V. cholerae* C6706 host and therefore has become an ideal model system to study the regulatory principles underlying QS-mediated phage induction.^{8,9,35}

To better understand the interplay between VP882 and *V. cholerae*, we recorded the transcriptomes of VP882 and *V. cholerae* before (lysogenic state) and at several time points (15, 60, and 120 min) after phage induction with DPO. We employed a *tdh*-deficient *V. cholerae* strain in these experiments to exclude endogenous DPO production.¹⁴ When compared with a non-treated control sample, the addition of DPO did not significantly affect cell growth within the first 60 min after treatment, however, strongly impaired growth further on (Figure 1B). This phenotype also correlated with a reduction in colony-forming units (CFUs), and we note that ~1%–2% of all cells did not engage in cell lysis upon phage activation (Figure S1A). Conversely, VP882 induction resulted in strongly elevated extracellular phage DNA levels and upregulation of the relative proportion of phage-specific reads in the transcriptomic datasets (Figures 1C and S1A). Specifically, we discovered that ~3%–5% of the reads mapped to the VP882 genome before and 15 min after the addition of DPO, whereas ~20%–25% of the reads were phage-specific at the 60 and 120 min time points. Detailed inspection of the phage genes revealed that nearly all genes were activated by DPO treatment at these time points; however, only a few changes were observed 15 min after the addition of DPO (Figure 1D). One notable exception was the *qtip* gene, displaying ~2.4-fold induction when compared with the pre-induction state. This observation is in line with the hierarchical organization underlying DPO-mediated induction of VP882, since activation of the VqmA_{phage} receptor by DPO triggers Qtip synthesis, which in turn sequesters and deactivates the CI repressor protein resulting in phage activation (Figure 1A).⁹ We also detected differentially expressed host genes in

response to VP882 activation. In accordance with the pattern observed for VP882, only a few genes (19) displayed differential expression 15 min after DPO treatment, whereas 1,384 and 1,949 were changed at the 60 and 120 min time points, respectively (Figures 1E and S1B). Among the differentially regulated host genes, we discovered that VP882 induction resulted in the activation of genes located in the superintegron on chromosome 2 of the *V. cholerae* C6706 genome, whereas the levels of many non-coding RNAs were reduced under this condition (Figures 1E, S1C, and S1D).

To follow up on the differential expression of non-coding RNAs following VP882 activation, we classified the downregulated RNAs according to their documented roles in the cell (Figure S1E). We discovered that a large fraction (~50%) of the repressed non-coding RNAs belonged to the group of Hfq-binding sRNAs that are well known to modulate gene expression in *V. cholerae* and other bacteria.^{17,36,37} To confirm these results, we probed the expression of the previously reported Hfq-dependent sRNAs VqmR, FarS, CarZ, and Vcr017 on northern blots. In line with the transcriptomic data, we found that FarS, CarZ, and Vcr017 were all downregulated when VP882 was activated (Figure 1F). Expression of VqmR was initially induced due to the presence of DPO^{14,15}; however, the levels of the sRNA declined in later stages of phage induction. In contrast, the expression of the Hfq-independent Vcr068 sRNA¹⁵ remained stable throughout the experiment. Interestingly, plasmid-borne Hfq overexpression during VP882 activation resulted in elevated VqmR, FarS, CarZ, and Vcr017 levels, when compared with a control plasmid (Figure S1F). Taken together, we conclude that activation of VP882 by DPO strongly affects the transcriptomic output of *V. cholerae* including the downregulation of Hfq-dependent sRNAs.

RIP-seq analysis detects host- and phage-encoded Hfq-binding sRNAs

Hfq is an RNA chaperone best known to facilitate the interaction between two base-pairing transcripts.³⁸ Binding to Hfq also protects sRNAs from ribonucleolytic decay and given the limiting role of intracellular Hfq concentrations for sRNA activity,^{39–41} we speculated that VP882-derived transcripts might compete with cellular sRNAs for Hfq binding upon phage activation. To test this hypothesis, we determined the levels of Hfq protein before and after VP882 induction by DPO and monitored VP882 activation in wild-type and *hfq*-deficient *V. cholerae*. We discovered that Hfq levels were mildly upregulated 30 min after VP882 induction and returned to pre-induction levels at the 120 min time point (Figures 2A and S2A). When compared with their isogenic wild-type cells, lack of *hfq* resulted in accelerated cell lysis by VP882 (Figure S2B), supporting the idea that Hfq and Hfq-binding transcripts are involved in VP882 activation.

To better understand the roles of Hfq during VP882 induction, we next determined and quantified the RNA ligands of Hfq before and after phage activation (60 min time point). To this end, we performed RNA co-immunoprecipitation of Hfq-bound transcripts using *V. cholerae* cells carrying a 3XFLAG epitope at the C terminus of the chromosomal *hfq* gene and employed a *V. cholerae* strain lacking the 3XFLAG epitope as a negative control.²² Comparison of the abundances of individual Hfq-binding sRNAs (analogous to Figure 1, i.e., CarZ, FarS, and Vcr017)

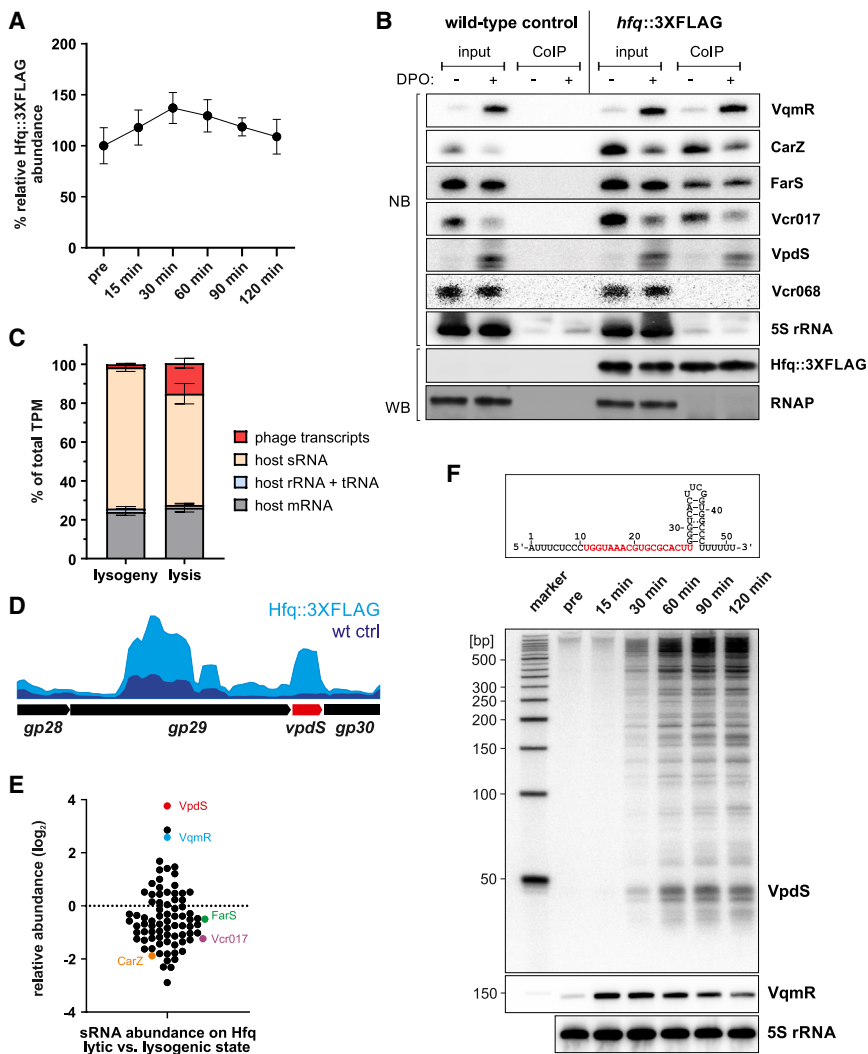


Figure 2. RIP-seq analysis detects host- and phage-encoded Hfq-binding sRNAs

(A) Quantification of Hfq levels during VP882 activation. Total protein samples of *V. cholerae* Δ *tad* cells carrying a chromosomal 3XFLAG epitope at the *hfq* gene lysogenized with VP882 were taken at indicated time points and analyzed by western blotting. Relative Hfq abundance was normalized to the RNAP loading control and was set to 100% (before induction; pre). The \pm SD of three biological replicates is indicated.

(B) RNA-coimmunoprecipitation (coIP) and total RNA fractions were obtained from *V. cholerae* Δ *tad* *hfq*::3XFLAG cells lysogenized with VP882. Cells were grown to OD₆₀₀ 0.4, back diluted 1:10 in M9 medium plus 0.035% arabinose and treated at OD₆₀₀ 0.2 for 60 min with H₂O (ctrl) or 25 μ M DPO. An untagged Δ *tad* strain (wild-type control) served as a negative control. RNA and protein fractions were separated and analyzed by northern (NB) and western blotting (WB), respectively. Northern blots were probed for indicated sRNAs. Ribosomal 5S RNA and RNAP served as loading controls.

(C) Relative TPM counts of Hfq coIP libraries obtained from lysogenic (water control) and lytic cultures (25 μ M DPO) 60 min post phage induction. TPM values were assigned to the origin of the RNA (host sRNAs, host rRNAs and tRNAs, host mRNAs, and phage transcripts) and normalized to the total TPM value of each cDNA library. Bars show the mean of independent biological replicates \pm SD, n = 3.

(D) Representative coverage plots of reads mapping to the IGR of the *gp28* and *gp30* genes 60 min post VP882 induction, comparing the untagged (wild type) and Hfq::3XFLAG-tagged strain.

(E) Changes in Hfq occupancy of Hfq-dependent sRNAs before and 60 min after VP882 activation. TPM values of each sRNA were normalized to the lysogenic state (set to 0). Higher and lower values indicate an increase or decrease in sRNA levels, respectively. Colored sRNAs were further validated by co-immunoprecipitation experiments (see B).

(F) Top panel: nucleotide sequence and predicted secondary structure of VpdS. The used oligo-probe for VpdS recognizes the red-marked nucleotide sequence. Lower panel: *V. cholerae* Δ *tad* cells lysogenized with VP882 were grown to OD₆₀₀ 0.4, diluted 1:10 in M9 medium plus 0.035% arabinose, and treated with 25 μ M DPO at OD₆₀₀ 0.2 (pre). At indicated time points, total RNA was collected and subjected to northern blotting to determine VpdS and VqmR levels by using anti-sense oligo probes KPO-8266 and KPO-0452, respectively. Ribosomal 5S RNA served as loading control.

See also Figure S2.

before and after DPO treatment revealed reduced sRNA levels after Hfq co-immunoprecipitation, whereas VqmR levels were increased following DPO treatment (Figure 2B). In accordance with these data, the activity of a *vqmR* transcriptional reporter was upregulated upon phage activation; however, analogous transcriptional reporters of the *vcr017* and *vcr068* genes displayed no significant change in activity (Figure S2C).

To test whether other Hfq-binding sRNAs also displayed reduced Hfq occupancy upon phage activation and to identify putative phage-derived transcript interacting with Hfq, we employed RNA sequencing to determine Hfq-associated transcripts at a global scale. Quantification of Hfq-bound transcripts according to their genomic origin revealed that only ~2% of all sequencing reads mapped to the VP882 genome in the lysogenic state, however, this number was increased to ~15% when the phage was induced (Figure 2C). Importantly, while

the percentage of host mRNAs, rRNAs, and tRNAs binding to Hfq remained constant before and after DPO treatment, the relative proportion of host sRNAs was reduced when VP882 was induced. These data suggest that VP882-derived transcripts occupy a significant proportion of Hfq after phage induction, which outcompete host-encoded sRNAs.

The VP882 genome contains 71 putative open reading frames (ORFs)⁴²; and using dRNA-seq we annotated 59 transcriptional start sites (TSS) on the phage genome (Table S1). To study the binding of phage transcripts to Hfq, we compared the relative abundances of Hfq-bound sequencing reads before and after VP882 induction and searched for unannotated transcripts that could constitute Hfq-binding sRNAs (Figure S2D). Indeed, we discovered a potential sRNA in the 3' UTR of the *gp29* gene (encoding putative tail tube protein), which was enriched in the Hfq co-immunoprecipitation samples (Figure 2D). We named this

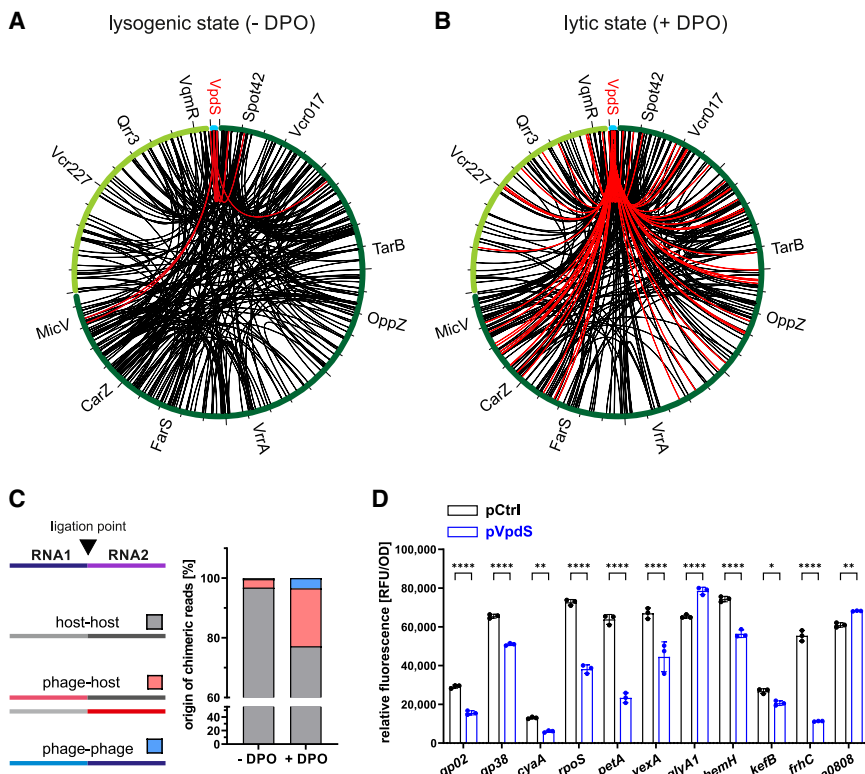


Figure 3. The host-phage interactome during the lysogenic and lytic lifestyle of VP882

(A and B) Circos plots visualizing the top 250 Hfq-associated RNA-RNA chimeras (FDR p value ≤ 0.05). *V. cholerae* hfq::3XFLAG cells lysogenized with VP882 were treated either with water (A), or 25 μ M DPO (B) to induce VP882 and subjected to RIL-seq analysis. The dark and light green colors indicate the large and small chromosomes of *V. cholerae*, respectively. The VP882 genome is marked in blue. Abundant sRNAs are indicated. The RNA-RNA interactome involving the VpdS sRNA is highlighted in red.

(C) Quantification of different chimeric fragments dependent on their genomic origin.

(D) Validation of VpdS-mRNA interactions identified by RIL-seq. Translational GFP reporter fusions were co-transformed with a constitutive sRNA expression plasmid or an empty control plasmid in *E. coli* top 10 cells. GFP production was measured and normalized to the respective OD. Bars show the mean of independent biological replicates \pm SD, $n = 3$. For statistical analyses, a two-way ANOVA with Bonferroni's multiple comparison test was used (* $p \leq 0.05$, ** $p \leq 0.01$, *** $p \leq 0.0001$). See also Figure S3.

transcript VpdS and confirmed its interaction with Hfq (Figure 2B, 5th panel from top). When compared with other Hfq-binding sRNAs, VpdS showed the strongest increase in Hfq occupancy of all sRNAs (Figure 2E), constituting $\sim 1.4\%$ of all reads mapping to Hfq-binding sRNAs (Figure S2E).

Our transcriptomic data together with northern blot analysis revealed that VpdS accumulates as a ~ 50 nucleotides long transcript and is first detectable 30 min following phage activation (Figures 1D and 2F). However, our dRNA-seq analysis did not report a TSS associated with *vpdS* (Table S1), suggesting the sRNA might be processed. We speculated that the major endoribonuclease RNase E might be involved in VpdS processing as it has previously been reported to cleave sRNAs from the 3' UTR of mRNAs.⁴³ To test this hypothesis, we expressed the *gp29* ORF including the 3' UTR from the inducible pBAD promoter on a plasmid and tested VpdS expression in a wild-type and a temperature-sensitive RNase E mutant (*rne*^{TS}).⁴⁴ Northern blot analysis revealed that the *rne*^{TS} mutant failed to produce the mature VpdS sRNA under non-permissive temperatures (44°C), whereas VpdS maturation was intact in wild-type cells (Figure S2F). In summary, our data suggest that both Hfq and RNase E are involved in the binding and processing of phage transcripts and that VpdS is an Hfq-associated phage sRNAs that is produced during VP882 activation.

Global identification of RNA-RNA interactions during phage lysogeny and lysis

In the past few years, several new technologies have been developed to detect RNA duplex formation at a genome-wide scale.^{45,46} One of these technologies is RNA interaction by ligation and sequencing (RIL-seq), which relies on cross-linking of

two RNAs on Hfq, followed by RNA ligation, cDNA generation, and sequencing of the chimeric reads.⁴⁷ We have previously established RIL-seq in *V. cholerae* revealing hundreds of Hfq-mediated interactions.²³ Therefore, we used RIL-seq to globally determine RNA duplex formation between host- and VP882-encoded transcripts. Following the experimental setup from above, we obtained RIL-seq samples from *V. cholerae* cells harboring VP882 in the lysogenic state and after phage induction by DPO (60 min time point). We detected a total of 1,297 and 1,975 interactions from the lysogenic and lytic states, respectively, and discovered a strong shift toward RNA duplexes involving phage-derived transcripts in the lytic state (Figures 3A and 3B). Classification of these interactions into three main categories, i.e., (1) interactions involving two host transcripts, (2) interactions containing one host and one phage transcripts, and (3) interactions between two phage transcripts, revealed that in the lysogenic state only few ($\sim 3\%$) RNA duplexes involved at least one phage transcript (Figure 3C; categories 2 and 3), whereas VP882 activation resulted in a strong increase in interactions containing phage RNA ($\sim 23\%$).

Our data also revealed a shift in the number of interacting targets for several host-encoded sRNAs and an increased number of interactions involving VpdS (Figures 3A, 3B, and S3A). Specifically, we discovered three interactions containing VpdS in the lysogenic state and 46 interactions after phage induction. Of note, these potential interaction partners involved host transcripts (Figure 3C, category 2), as well phage transcripts (e.g., *gp02* and *gp38*; category 3). To confirm post-transcriptional regulation of target mRNAs by VpdS, we focused on 11 putative targets (9 host and 2 phage genes, respectively) for which we were able to predict RNA duplex formation with VpdS (Figures S3B–S3L). We cloned the 5' UTRs of

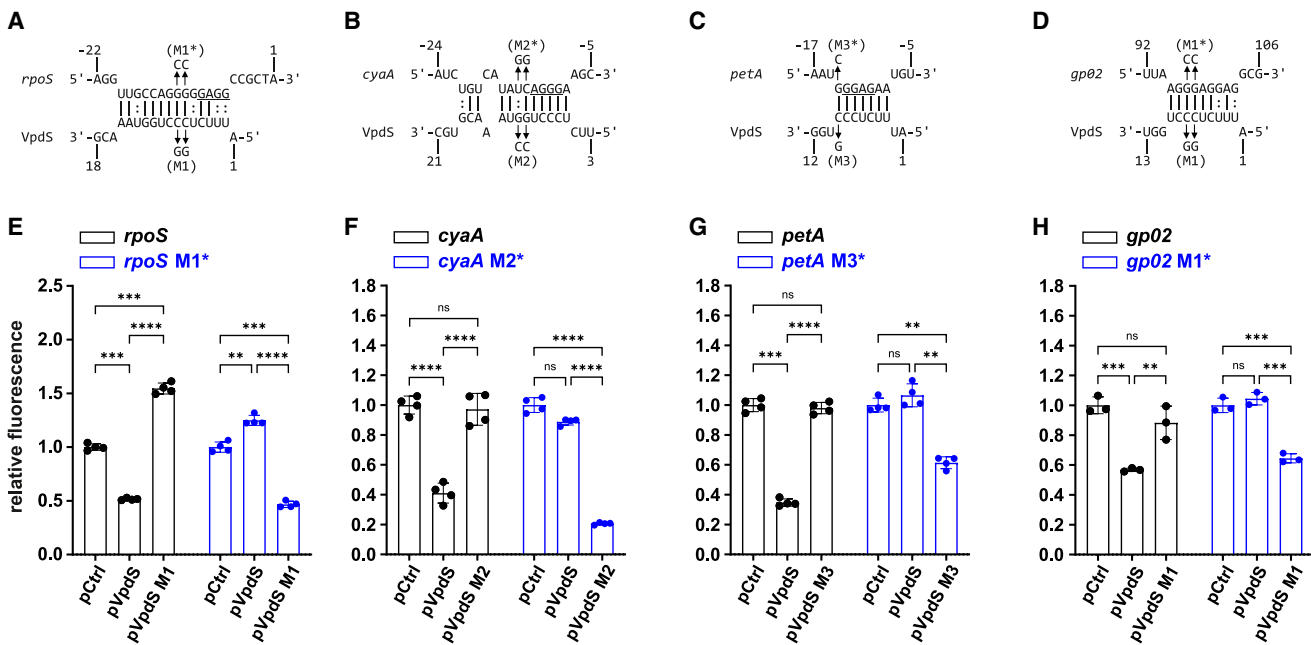


Figure 4. VpdS acts post-transcriptionally to modulate host and phage gene expression

(A–D) RNA duplex formation of VpdS with several target mRNAs. The putative Shine-Dalgarno sequence is underlined in the mRNA. Numbers denote the nucleotide position (5'-3') of the sRNA from the TSS and the start codons of the target mRNA sequence.

(E-H) Fluorescence intensities of *E. coli* strains carrying the gene-specific translational GFP reporters and the control plasmid (pCtrl) or the VpdS expression plasmid. The fluorescence intensity of the strains harboring the control plasmid was set to 1. Bars show the mean of at least three biological replicates \pm SD. For statistical analyses, a two-way ANOVA with Bonferroni's multiple comparison test was used (* $p \leq 0.01$, ** $p \leq 0.001$, *** $p \leq 0.0001$).

See also Figure S4.

these targets together with their initial coding sequence into a GFP-based reporter system and tested the effect of VpdS in *E. coli*. All targets displayed altered GFP expression in the presence of VpdS ranging from modest upregulation (e.g., *vca0808*) to ~6-fold downregulation for *frhC* (Figure 3D). In contrast, VpdS failed to regulate these targets (except *kefB*) in the absence of *hfq* (Figure S3M). These results suggest that VP882-encoded transcripts become involved in Hfq-mediated gene regulation upon phage activation and that VpdS is an abundant sRNA under this condition, regulating multiple target mRNAs in the host and the phage.

Interaction of VpdS with target mRNAs

Base-pairing sRNAs that act in concert with Hfq frequently employ single-stranded sequence elements to identify their target transcripts.⁴⁸ To determine the base-pairing sequence in VpdS that allows target recognition, we focused on four target transcripts (*rpoS*, *cyaA*, *petA*, and *gp02*) that were regulated in our reporter assay (Figure 3D). The *rpoS*, *cyaA*, and *petA* genes are located on the host genome and have previously been implicated in host-phage interactions,^{49–51} whereas *gp02* is a VP882 gene encoding the small terminase subunit required for DNA packaging.⁴² We predicted RNA duplex formation of VpdS with the four targets (Figures 4A–4D), which in all cases involved sequences at the 5' end of the sRNA (Figure S4A). To test these predictions, we generated three VpdS mutants (M1–M3; Figures 4A–4D and S4A) and examined their expression by northern blotting (Figure S4B). Although all VpdS mutant variants

were equally expressed, they failed to inhibit the expression of their respective targets (Figures 4E–4H). Mutation of the corresponding base pairs in the GFP reporters abrogated repression by wild-type VpdS, however, when combined with the respective VpdS variant, regulation was restored. Of note, whereas regulation of the three host genes all involved sequestration of the target ribosome-binding site (Figures 4A–4C), regulation of *gp02* occurs in the coding sequence (Figure 4D), indicating that target regulation might be accompanied by ribonuclease recruitment.⁵² To link regulation of these reporters by VpdS to protein production in *V. cholerae*, we added a 3XFLAG epitope to the chromosomal *rpoS* and *cyaA* genes and tested regulation by VpdS on western blots. In accordance with the data obtained from the GFP reporters, production of RpoS::3XFLAG and CyaA::3XFLAG was reduced by VpdS, whereas no regulation was detected when VpdS M1 was expressed (Figure S4C). Taken together, these data suggest that VpdS is a bona fide Hfq-binding sRNA that controls gene expression by base-pairing with target mRNAs.

VpdS accelerates VP882 replication and host cell lysis

Hfq-binding sRNAs have important regulatory roles in many aspects of microbial physiology and virulence⁵³; however, their role during phage replication has not been explored, yet. The discovery of the *VpdS* sRNA allowed us to address this question in the context of VP882 activation by DPO. To this end, we generated a *vpdS* deletion mutant on the chromosome of VP882 by removing the base-pairing sequence of the sRNA (deleting bp 1–20 of the

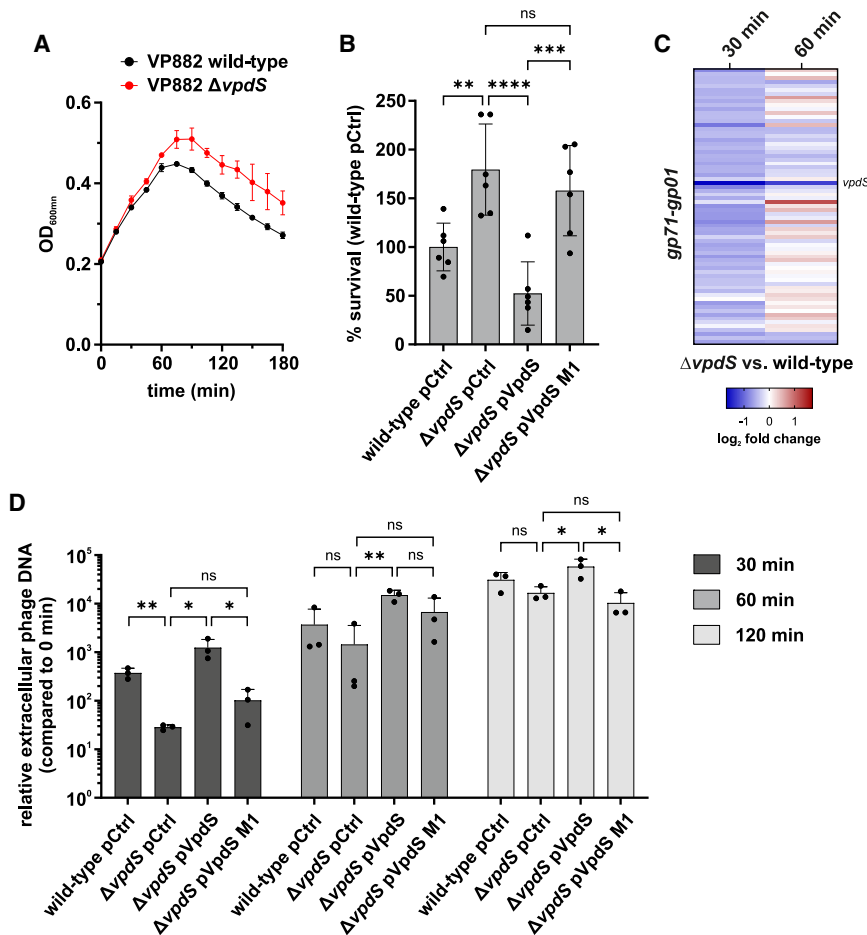


Figure 5. VpdS accelerates VP882 replication and host cell lysis

(A) Growth kinetics of *V. cholerae* Δtdh lysogenized with VP882 wild-type (black) or VP882 ΔvpdS (red) were grown to OD₆₀₀ 0.4, back diluted 1:10 in M9 medium plus 0.035% arabinose (pre, 0 min) and treated at OD₆₀₀ 0.2 with 25 μM DPO. Dots show the mean of independent biological replicates ± SD, n = 3.

(B) *V. cholerae* carrying the indicated phage variants and plasmids (x axis) were cultivated as described above. Survival was determined 60 min post VP882 induction by counting colony-forming units (CFUs). Bars represent the mean of six independent biological replicates ± SD. Statistical significance was determined using one-way ANOVA and Sídák's multiple comparisons test.

(C) Heatmap of transcriptome changes in VP882 in response to DPO-mediated phage activation. Viral gene expression is represented as a log₂ fold difference comparing VP882 ΔvpdS with wild-type VP882 30 and 60 min post induction. The *vpdS* gene is highlighted.

(D) Relative amount of extracellular viral DNA during the lytic life cycle of VP882. *V. cholerae* with indicated phage variants and plasmids (x axis) was grown as described above and extracellular DNA was quantified by qPCR. The DNA amount before treatment (0 min) was set to 1. Bars represent the mean of three independent biological replicates ± SD. Statistical significance was analyzed using an unpaired t test (*p ≤ 0.05, **p ≤ 0.01, ***p ≤ 0.0001, ****p ≤ 0.0001, ns, not significant).

See also Figure S5.

vpdS gene), while leaving the Rho-independent terminator intact (Figure S4A). When monitoring DPO-mediated cell lysis by VP882 wild-type and ΔvpdS phage, we noticed that both phages were able to induce cell lysis; however, this process was significantly delayed in the absence of *vpdS* (Figure 5A). In contrast, plasmid-borne VpdS overexpression resulted in reduced cell growth and accelerated cell lysis upon VP882 activation (Figure S5A).

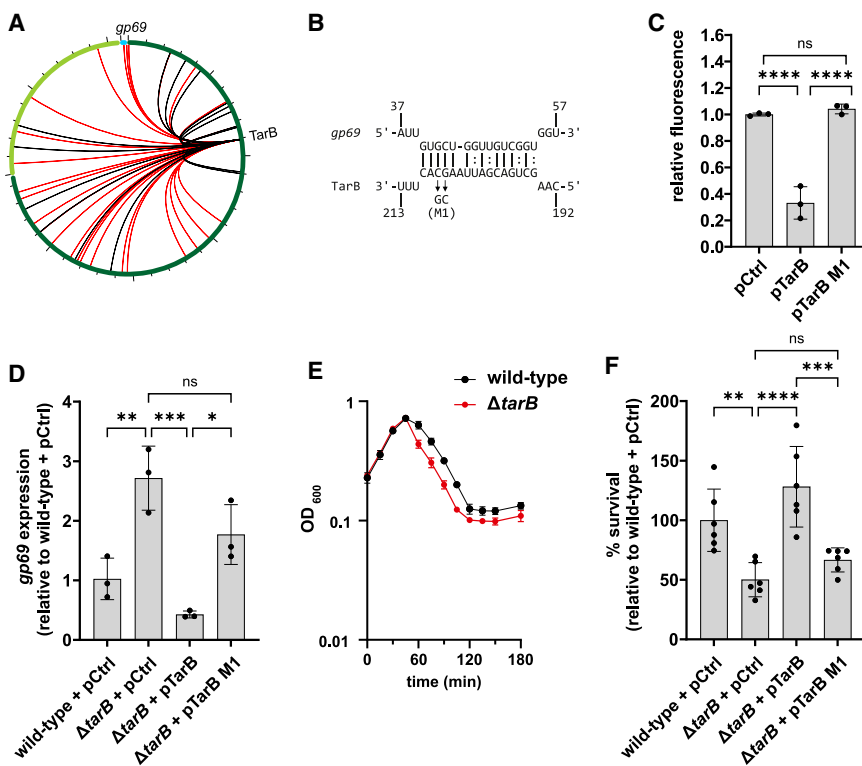
We next asked whether the difference in cell density between the wild-type VP882 and the *vpdS* mutant would also translate into changes in cell survival by counting CFUs before and after phage induction. Indeed, mutation of *vpdS* resulted in ~75% higher survival of *V. cholerae*, when compared with the wild-type phage (Figure 4B). In contrast, overexpression of VpdS reversed this phenotype (~50% decreased survival), whereas overexpression of the VpdS M1 mutant (unable to regulate *rpoS* and *gp02*; Figures 4E and 4H) failed to complement the ΔvpdS phenotype. Of note, all four strains displayed highly similar CFU counts under lysogeny conditions (Figure S5B).

To better understand the molecular underpinnings associated with *vpdS* deficiency in VP882, we used quantitative real-time PCR to monitor *gp02* mRNA levels in wild-type and ΔvpdS VP882 phage, as well as in the complementation strains. Mutation of *vpdS* resulted in increased *gp02* levels, whereas plasmid-borne VpdS expression showed the opposite effect (Figure S5C). Analogous to the CFU counts (Figure 5B), overexpres-

sion of VpdS M1 did not modulate *gp02* levels in the ΔvpdS mutant.

These results motivated us to also record the complete transcriptomes of *V. cholerae* cells harboring either the wild-type or ΔvpdS VP882 phage. Comparison of the host transcriptomes identified 100 and 175 deregulated host genes 30 and 60 min after the addition of DPO treatment, respectively (Figure S5D). Inspection of the phage transcriptome revealed downregulation of >60% of all phage genes (44/71) at the 30 min time point in the *vpdS* mutant, while only a few genes were differentially expressed 60 min following phage induction (Figure 5C). This pattern mirrored the initial delay in cell lysis detected in the *vpdS* mutant (Figure 5A) and suggested that VpdS is involved in the coordination of VP882 replication and assembly.

To test this hypothesis, we quantified the amount of extracellular VP882 DNA following DPO-mediated activation as a proxy for phage assembly. As expected, we detected a strong increase in phage DNA levels upon DPO treatment (Figure 5D). VP882 lacking *vpdS* produced ~10-fold less phage DNA than the isogenic wild-type phage at the 30 min time point; however, DNA levels were almost equal at later stages of phage induction. Overexpression of VpdS resulted in increased external phage DNA, while the VpdS M1 mutant failed to produce this effect (30 min time point). In summary, we conclude that VpdS expression facilitates the phage replication and lysis process through base-pairing with target mRNAs.



normalized to the house-keeping gene *recA*. Bars show relative *gp69* expression of three biologically independent replicates \pm SD compared with wild type. Statistical significance was calculated by using one-way ANOVA and Šídák's multiple comparisons test. (E) Synchronized cultures at OD_{600} 0.2 were treated at OD_{600} 0.2 with 25 μ M DPO and 0.01% arabinose and the OD_{600} was monitored every 30 min. Dots show the mean of independent biological replicates \pm SD, $n = 3$. (F) Survival was determined 180 min post phage induction by counting colony-forming units (CFUs). Bars represent the mean of six biologically independent replicates \pm SD. Statistical significance was analyzed using one-way ANOVA and Šídák's multiple comparisons test (* $p \leq 0.05$, ** $p \leq 0.01$, *** $p \leq 0.001$, **** $p \leq 0.0001$, ns, not significant).

See also Figure S6.

TarB is a host sRNA that interferes with VP882 replication

The above data showed that transcripts from *V. cholerae* and VP882 form hundreds of RNA duplexes on Hfq and that VpdS is a phage-derived sRNA that promotes phage replication. Vice versa, we hypothesized that host-encoded sRNAs could base pair with phage transcripts to antagonize phage replication. To explore this idea, we searched the RIL-seq dataset for host sRNAs interacting with VP882-encoded mRNAs and found three candidate sRNAs (*VrrA*, *Vcr227*, and *TarB*) displaying a high number of putative interactions (Figure S6A). Among these, we focused on the *TarB* sRNA as it was found in several new RNA duplexes upon VP882 induction (Figure 6A).

One of these interactions involved the mRNA of *gp69*, encoding the first gene of the phage cell lysis operon⁴² (Figure S6B), suggesting that *TarB* might regulate VP882-mediated cell lysis. Northern blot analysis revealed that *TarB* is detectable throughout the VP882 replication process (Figure S6C). Of note, we detected two isoforms of *TarB* of which the shorter variant aligns with the annotated length of *TarB* (78 nucleotides; Bradley et al.²⁷). The longer isoform (240 nucleotides) employs the same Rho-independent terminator, however, uses a TSS located 162 bp further upstream.¹⁵ We confirmed that the larger *TarB* isoform is expressed in *V. cholerae* and inhibits the expres-

sion of the previously reported *tcpF* target (Figures S6D and S6E) and also tested regulation of *gp69*. Indeed, *TarB* efficiently inhibited a *gp69::gfp* reporter, and mutation of *TarB* (*TarB M1*) or *hfq* abrogated this effect (Figures 6B, 6C, and S6F).

Consequently, we monitored *gp69* mRNA expression in wild-type and $\Delta tarB$ *V. cholerae* cells during VP882 activation. Whereas mutation of *tarB* did not affect *gp69* levels in the lysogenic state (Figure S6G), DPO-mediated activation of VP882 in $\Delta tarB$ cells resulted in \sim 2.8-fold increased *gp69* levels, when compared with the isogenic wild-type strain (Figure 6D). In contrast, *TarB* over-production inhibited *gp69* expression and this effect was reduced for the mutated *TarB* variant.

We further corroborated these results by comparing growth curves and CFU counts in wild-type and $\Delta tarB$ cells before and after phage activation. Indeed, mutation of *tarB* resulted in accelerated cell lysis (Figure 6E). Analogous to VpdS (Figure S5A), *tarB* did not affect cell survival in the absence of DPO (Figure S6H); however, when VP882 was induced, $\Delta tarB$ cells displayed \sim 50% reduced CFUs compared to wild-type cells (Figure 6F). Plasmid-borne expression of *TarB* complemented this phenotype, while *TarB M1* had no significant effect on cell survival. Taken together, these data suggest that *TarB* counteracts phage replication by inhibiting the expression of the lysis gene operon.

DISCUSSION

The discovery of CRISPR-Cas and other anti-phage defense systems has sparked a renaissance in phage biology over the past few years.^{54,55} Whereas CRISPR-Cas systems employ anti-sense-guided crRNAs (CRISPR RNAs) to recognize and destroy foreign nucleic acids, other defense systems rely on protein-centered mechanisms to counteract phage replication.⁴ Cross-talk at the post-transcriptional level, i.e., through regulatory RNAs or RNA-binding proteins, also plays an important role in host-phage interactions, yet the associated regulatory processes are often less clear.^{56–60} Specifically, the majority of phage-derived sRNAs stem from inactive prophages that integrated into the host genome, making it difficult to determine whether the detected regulatory patterns are bona fide phage functions, or rather constitute adaptive co-evolutionary effects between the host and phage.³¹

The interaction of VP882 with *V. cholerae* is unique in the sense that the phage can be activated by a QS molecule (DPO) that does not trigger other lysogenic phages or host stress response systems, which could muddle the interpretation of the results. Interestingly, natural isolates harboring VP882 have been reported to carry mutations in QS-related genes, underscoring the central role of QS in the lifecycle of VP882.⁶¹ Further, VP882 can assemble in and lyse *V. cholerae* C6706; however, it fails to re-infect the host allowing us to obtain a time-resolved view of the phage activation process (Figures 1B–1E).⁹ It is currently unknown why VP882 is unable to infect *V. cholerae* C6706; however, it has been reported that VP882 can infect various other *Vibrio* strains⁴² (including *V. cholerae*), suggesting that our results are relevant under natural conditions.

VP882 belongs to the growing class of plasmid phages that are frequent in Enterobacteria and recently have been implicated in the spread of antibiotic resistance genes.^{33,62} VP882 induction relies on DPO and/or DNA damage⁹ resulting in strong transcriptional activation of nearly all phage genes, including *vpdS* (Figures 1D and 2F). Accumulation of *vpdS* requires processing of the *gp29-vpdS* transcript by RNase E, which is analogous to several host-encoded sRNAs that reside in the 3' UTR of mRNAs.⁴³ RNase E recognizes its substrates through conserved AUU motif downstream the cleavage site⁴⁴ that is also present in *vpdS* (Figure S4A). RNase E frequently acts in concert with Hfq,⁶³ supporting the idea that both Hfq-mediated RNA duplex formation and cleavage of phage transcripts by host-encoded ribonucleases are relevant for the interplay of VP882 with its host.

Similarly, eukaryotic viruses often rely on the post-transcriptional machinery of the host to establish an infection and/or overwhelm the immune response.⁶⁴ Analogous to the strong impact of VP882 activation on the pool of Hfq-binding partners in *V. cholerae* (Figures 2C, 2E, 3A, and 3B), viral infections have frequently been associated with a shift in microRNA signatures in the host.⁶⁵ For example, Epstein-Barr virus encodes 44 microRNAs that require the host's dicer-dependent maturation pathway and inhibit the expression of key immune pathways, such as the retinoic-acid-inducible gene I (RIG-I).⁶⁶ Conversely, host-encoded microRNAs have been shown to counteract virus infections in animals, plants, and humans, indicating a highly conserved defense strategy.⁶⁷ Our data indicate that bacteria also employ base-pairing regulators to antagonize viral replica-

tion and vice versa that phages tap into the post-transcriptional machinery of the host to modulate gene expression.

The target spectra of VpdS and TarB suggest that both sRNAs are capable of regulating host as well as phage genes (Figures 3B and 6A). Transcription of *tarB* is controlled by ToxT, and the sRNA has been reported to regulate several targets in *V. cholerae*, including genes that could facilitate its anti-viral activity.^{27,28} With respect to VP882, TarB seems to provide anti-phage activity by repressing the mRNAs of the phage lysis operon (Figure 6). Of note, the *tarB* gene is encoded on a horizontally acquired genomic island (VPI; Bradley et al.²⁷), which is a hallmark of many anti-phage genes.⁶⁸ In addition to TarB, several other host-encoded sRNAs might participate in phage defense, either through direct regulation of phage genes or by modulating the expression of stress genes that could help to counteract phage induction and cell lysis. This view is supported by our observation that *V. cholerae* *hfq* mutants displayed accelerated cell lysis upon VP882 induction (Figure S2B).

Likewise, the role of VpdS during VP882 activation might also involve the regulation of multiple target mRNAs from the host and the phage (Figure 4). Specifically, the *gp02* phage mRNA encodes a DNA-packing protein, and inhibition by VpdS could serve as a phage intrinsic regulatory process that helps to coordinate phage assembly. In contrast, regulation of *rpoS* by VpdS (Figure 4E) is more likely to indirectly promote VP882 replication. The *rpoS* gene encodes σ^S ,⁶⁹ an alternative sigma factor that activates several starvation genes and that could draw cellular resources away from the phage. In addition, σ^S -bound RNA polymerase is unlikely to recognize VP882 promoters, which could slow down phage replication. Indeed, VP882 mutants lacking *vpdS* display delayed cell lysis and reduced expression of phage genes (Figures 5A–5C). Intriguingly, T7 phage infecting *E. coli* has also been demonstrated to inhibit σ^S activity⁴⁹; however, this function is mediated by a protein (called Gp5.7), rather than a regulatory RNA. Of note, in addition to interfering with post-transcriptional regulation of its host, the VP882 genome also encodes a homolog of the TraR protein (Orf61) that has been reported to inhibit transcription at ribosomal promoters of the host.⁷⁰ Taken together, viruses and phages have developed complex mechanisms to subvert the host gene expression machinery involving both RNA- and protein-based regulation.

STAR★METHODS

Detailed methods are provided in the online version of this paper and include the following:

- KEY RESOURCES TABLE
- RESOURCE AVAILABILITY
 - Lead contact
 - Materials availability
 - Data and code availability
- EXPERIMENTAL MODEL AND SUBJECT DETAILS
 - Bacterial strains
- METHOD DETAILS
 - Plasmid construction
 - RNA isolation, Northern blot analysis and quantitative real-time PCR
 - Western blot analysis and fluorescence assays

- Generation of phage mutant strains
- Phage DNA preparation and quantitative PCR
- RNAseq and dRNAseq VP882 activation
- Hfq coimmunoprecipitation and RIP-seq analysis
- Hfq RIL-seq and computational analysis
- RNA-seq analysis of VP882 wild-type and VP882 Δ vpdS

● QUANTIFICATION AND STATISTICAL ANALYSIS

SUPPLEMENTAL INFORMATION

Supplemental information can be found online at <https://doi.org/10.1016/j.chom.2024.03.010>.

ACKNOWLEDGMENTS

We thank Andreas Starick and Yvonne Greiser for their excellent technical support. We thank Jörg Vogel and Kathrin Fröhlich for their comments on the manuscript and all members of the Papenfort lab for insightful discussions and suggestions. This work was supported by the German Research Foundation (SPP2330, project-ID 464459808 and EXC 2051, project-ID 390713860), the Vallee Foundation (to K.P.), and the European Research Council (ArtRNA, CoG-101088027).

AUTHOR CONTRIBUTIONS

Conceptualization, M. Sprenger and K.P.; methodology, M. Sprenger; investigation, M. Sprenger and M. Siemers; formal analysis, M. Sprenger and M. Siemers; data curation, M. Sprenger, M. Siemers, and S.K.; writing – original draft, M. Sprenger and K.P.; writing – review & editing, M. Sprenger and K.P.; visualization, M. Sprenger, M. Siemers, and S.K.; funding acquisition, K.P.

DECLARATION OF INTERESTS

The authors declare no competing interests.

Received: November 21, 2023

Revised: February 2, 2024

Accepted: March 13, 2024

Published: April 4, 2024

REFERENCES

1. Hatfull, G.F. (2015). Dark Matter of the Biosphere: the Amazing World of Bacteriophage Diversity. *J. Virol.* **89**, 8107–8110. <https://doi.org/10.1128/JVI.01340-15>.
2. Clokie, M.R., Millard, A.D., Letarov, A.V., and Heaphy, S. (2011). Phages in nature. *Bacteriophage* **1**, 31–45. <https://doi.org/10.4161/bact.1.1.14942>.
3. Slavik, K.M., and Kranzusch, P.J. (2023). CBASS to cGAS-STING: The Origins and Mechanisms of Nucleotide Second Messenger Immune Signaling. *Annu. Rev. Virol.* **10**, 423–453. <https://doi.org/10.1146/annurev-virology-111821-115636>.
4. Georjon, H., and Bernheim, A. (2023). The highly diverse antiphage defence systems of bacteria. *Nat. Rev. Microbiol.* **21**, 686–700. <https://doi.org/10.1038/s41579-023-00934-x>.
5. Huiting, E., Cao, X., Ren, J., Athukoralage, J.S., Luo, Z., Silas, S., An, N., Carion, H., Zhou, Y., Fraser, J.S., et al. (2023). Bacteriophages inhibit and evade cGAS-like immune function in bacteria. *Cell* **186**, 864–876.e21. <https://doi.org/10.1016/j.cell.2022.12.041>.
6. León-Félix, J., and Villicaña, C. (2021). The impact of quorum sensing on the modulation of phage-host interactions. *J. Bacteriol.* **203**, e00687–20. <https://doi.org/10.1128/JB.00687-20>.
7. Erez, Z., Steinberger-Levy, I., Shamir, M., Doron, S., Stokar-Avihail, A., Peleg, Y., Melamed, S., Leavitt, A., Savidor, A., Albeck, S., et al. (2017). Communication between viruses guides lysis-lysogeny decisions. *Nature* **541**, 488–493. <https://doi.org/10.1038/nature21049>.
8. Silpe, J.E., Bridges, A.A., Huang, X., Coronado, D.R., Duddy, O.P., and Bassler, B.L. (2020). Separating Functions of the Phage-Encoded Quorum-Sensing-Activated Antirepressor Qtip. *Cell Host Microbe* **27**, 629–641.e4. <https://doi.org/10.1016/j.chom.2020.01.024>.
9. Silpe, J.E., and Bassler, B.L. (2019). A Host-Produced Quorum-Sensing Autoinducer Controls a Phage Lysis-Lysogeny Decision. *Cell* **176**, 268–280.e13. <https://doi.org/10.1016/j.cell.2018.10.059>.
10. Stokar-Avihail, A., Tal, N., Erez, Z., Lopatina, A., and Sorek, R. (2019). Widespread Utilization of Peptide Communication in Phages Infecting Soil and Pathogenic Bacteria. *Cell Host Microbe* **25**, 746–755.e5. <https://doi.org/10.1016/j.chom.2019.03.017>.
11. Silpe, J.E., Duddy, O.P., Johnson, G.E., Beggs, G.A., Hussain, F.A., Forsberg, K.J., and Bassler, B.L. (2023). Small protein modules dictate prophage fates during polylysogeny. *Nature* **620**, 625–633. <https://doi.org/10.1038/s41586-023-06376-y>.
12. Silpe, J.E., and Bassler, B.L. (2019). Phage-Encoded LuxR-Type Receptors Responsive to Host-Produced Bacterial Quorum-Sensing Autoinducers. *mBio* **10**, e00638–19. <https://doi.org/10.1128/mBio.00638-19>.
13. Silpe, J.E., Duddy, O.P., and Bassler, B.L. (2022). Natural and synthetic inhibitors of a phage-encoded quorum-sensing receptor affect phage-host dynamics in mixed bacterial communities. *Proc. Natl. Acad. Sci. USA* **119**, e2217813119. <https://doi.org/10.1073/pnas.2217813119>.
14. Papenfort, K., Silpe, J.E., Schramma, K.R., Cong, J.-P., Seyedsayamdst, M.R., and Bassler, B.L. (2017). A *Vibrio cholerae* autoinducer–receptor pair that controls biofilm formation. *Nat. Chem. Biol.* **13**, 551–557. <https://doi.org/10.1038/nchembio.2336>.
15. Papenfort, K., Förstner, K.U., Cong, J.P., Sharma, C.M., and Bassler, B.L. (2015). Differential RNA-seq of *Vibrio cholerae* identifies the VqmR small RNA as a regulator of biofilm formation. *Proc. Natl. Acad. Sci. USA* **112**, E766–E775. <https://doi.org/10.1073/pnas.1500203112>.
16. Herzog, R., Peschek, N., Fröhlich, K.S., Schumacher, K., and Papenfort, K. (2019). Three autoinducer molecules act in concert to control virulence gene expression in *Vibrio cholerae*. *Nucleic Acids Res.* **47**, 3171–3183. <https://doi.org/10.1093/nar/gky1320>.
17. Kavita, K., de Mets, F., and Gottesman, S. (2018). New aspects of RNA-based regulation by Hfq and its partner sRNAs. *Curr. Opin. Microbiol.* **42**, 53–61. <https://doi.org/10.1016/j.mib.2017.10.014>.
18. Franze de Fernandez, M.T., Eoyang, L., and August, J.T. (1968). Factor fraction required for the synthesis of bacteriophage Qbeta-RNA. *Nature* **219**, 588–590. <https://doi.org/10.1038/21958a0>.
19. Chao, Y., and Vogel, J. (2010). The role of Hfq in bacterial pathogens. *Curr. Opin. Microbiol.* **13**, 24–33. <https://doi.org/10.1016/j.mib.2010.01.001>.
20. Ding, Y., Davis, B.M., and Waldor, M.K. (2004). Hfq is essential for *Vibrio cholerae* virulence and downregulates sigma expression. *Mol. Microbiol.* **53**, 345–354. <https://doi.org/10.1111/j.1365-2958.2004.04142.x>.
21. Lenz, D.H., Mok, K.C., Lilley, B.N., Kulkarni, R.V., Wingreen, N.S., and Bassler, B.L. (2004). The small RNA chaperone Hfq and multiple small RNAs control quorum sensing in *Vibrio harveyi* and *Vibrio cholerae*. *Cell* **118**, 69–82. <https://doi.org/10.1016/j.cell.2004.06.009>.
22. Huber, M., Fröhlich, K.S., Radmer, J., and Papenfort, K. (2020). Switching fatty acid metabolism by an RNA-controlled feed forward loop. *Proc. Natl. Acad. Sci. USA* **117**, 8044–8054. <https://doi.org/10.1073/pnas.1920753117>.
23. Huber, M., Lippegaus, A., Melamed, S., Siemers, M., Wucher, B.R., Hoyos, M., Nadell, C., Storz, G., and Papenfort, K. (2022). An RNA sponge controls quorum sensing dynamics and biofilm formation in *Vibrio cholerae*. *Nat. Commun.* **13**, 7585. <https://doi.org/10.1038/s41467-022-35261-x>.
24. Venkat, K., Hoyos, M., Haycocks, J.R., Cassidy, L., Engelmann, B., Rolle-Kampczyk, U., von Bergen, M., Tholey, A., Grainger, D.C., and Papenfort, K. (2021). A dual-function RNA balances carbon uptake and central

- metabolism in *Vibrio cholerae*. *EMBO J.* 40, e108542. <https://doi.org/10.15252/embj.2021108542>.
25. Song, T., Mika, F., Lindmark, B., Liu, Z., Schild, S., Bishop, A., Zhu, J., Camilli, A., Johansson, J., Vogel, J., and Wai, S.N. (2008). A new *Vibrio cholerae* sRNA modulates colonization and affects release of outer membrane vesicles. *Mol. Microbiol.* 70, 100–111. <https://doi.org/10.1111/j.1365-2958.2008.06392.x>.
 26. Peschek, N., Hoyos, M., Herzog, R., Förstner, K.U., and Papenfort, K. (2019). A conserved RNA seed-pairing domain directs small RNA-mediated stress resistance in enterobacteria. *EMBO J.* 38, e101650. <https://doi.org/10.15252/embj.2019101650>.
 27. Bradley, E.S., Bodí, K., Ismail, A.M., and Camilli, A. (2011). A genome-wide approach to discovery of small RNAs involved in regulation of virulence in *Vibrio cholerae*. *PLoS Pathog.* 7, e1002126. <https://doi.org/10.1371/journal.ppat.1002126>.
 28. Davies, B.W., Bogard, R.W., Young, T.S., and Mekalanos, J.J. (2012). Coordinated regulation of accessory genetic elements produces cyclic di-nucleotides for *V. cholerae* virulence. *Cell* 149, 358–370. <https://doi.org/10.1016/j.cell.2012.01.053>.
 29. Richard, A.L., Withey, J.H., Beyhan, S., Yıldız, F., and DiRita, V.J. (2010). The *Vibrio cholerae* virulence regulatory cascade controls glucose uptake through activation of TarA, a small regulatory RNA. *Mol. Microbiol.* 78, 1171–1181. <https://doi.org/10.1111/j.1365-2958.2010.07397.x>.
 30. Kumar, A., Das, B., and Kumar, N. (2020). *Vibrio* Pathogenicity Island-1: The Master Determinant of Cholera Pathogenesis. *Front. Cell. Infect. Microbiol.* 10, 561296. <https://doi.org/10.3389/fcimb.2020.561296>.
 31. Altuvia, S., Storz, G., and Papenfort, K. (2018). Cross-Regulation between Bacteria and Phages at a Posttranscriptional Level. *Microbiol. Spectr.* 6, 10. <https://doi.org/10.1128/microbiolspec.RWR-0027-2018>.
 32. Fröhlich, K.S., and Papenfort, K. (2016). Interplay of regulatory RNAs and mobile genetic elements in enteric pathogens. *Mol. Microbiol.* 101, 701–713. <https://doi.org/10.1111/mmi.13428>.
 33. Pfeifer, E., Moura de Sousa, J.A., Touchon, M., and Rocha, E.P.C. (2021). Bacteria have numerous distinctive groups of phage-plasmids with conserved phage and variable plasmid gene repertoires. *Nucleic Acids Res.* 49, 2655–2673. <https://doi.org/10.1093/nar/gkab064>.
 34. Silpe, J.E., Duddy, O.P., and Bassler, B.L. (2023). Induction mechanisms and strategies underlying interphage competition during polylysogeny. *PLoS Pathog.* 19, e1011363. <https://doi.org/10.1371/journal.ppat.1011363>.
 35. Duddy, O.P., Huang, X., Silpe, J.E., and Bassler, B.L. (2021). Mechanism underlying the DNA-binding preferences of the *Vibrio cholerae* and vibriophage VP882 VqmA quorum-sensing receptors. *PLoS Genet.* 17, e1009550. <https://doi.org/10.1371/journal.pgen.1009550>.
 36. Ghandour, R., and Papenfort, K. (2023). Small regulatory RNAs in *Vibrio cholerae*. *Microlife* 4, uquad030. <https://doi.org/10.1093/femsml/uquad030>.
 37. Quendera, A.P., Seixas, A.F., Dos Santos, R.F., Santos, I., Silva, J.P.N., Arraiano, C.M., and Andrade, J.M. (2020). RNA-Binding Proteins Driving the Regulatory Activity of Small Non-coding RNAs in Bacteria. *Front. Mol. Biosci.* 7, 78. <https://doi.org/10.3389/fmbo.2020.00078>.
 38. Santiago-Frangos, A., and Woodson, S.A. (2018). Hfq chaperone brings speed dating to bacterial sRNA. *Wiley Interdiscip. Rev. RNA* 9, e1475. <https://doi.org/10.1002/wrna.1475>.
 39. Moon, K., and Gottesman, S. (2011). Competition among Hfq-binding small RNAs in *Escherichia coli*. *Mol. Microbiol.* 82, 1545–1562. <https://doi.org/10.1111/j.1365-2958.2011.07907.x>.
 40. Hussein, R., and Lim, H.N. (2011). Disruption of small RNA signaling caused by competition for Hfq. *Proc. Natl. Acad. Sci. USA* 108, 1110–1115. <https://doi.org/10.1073/pnas.1010082108>.
 41. Papenfort, K., Said, N., Welsink, T., Lucchini, S., Hinton, J.C.D., and Vogel, J. (2009). Specific and pleiotropic patterns of mRNA regulation by ArcZ, a conserved, Hfq-dependent small RNA. *Mol. Microbiol.* 74, 139–158. <https://doi.org/10.1111/j.1365-2958.2009.06857.x>.
 42. Lan, S.F., Huang, C.H., Chang, C.H., Liao, W.C., Lin, I.H., Jian, W.N., Wu, Y.G., Chen, S.Y., and Wong, H.C. (2009). Characterization of a new plasmid-like prophage in a pandemic *Vibrio parahaemolyticus* O3:K6 strain. *Appl. Environ. Microbiol.* 75, 2659–2667. <https://doi.org/10.1128/AEM.02483-08>.
 43. Ponath, F., Hörl, J., and Vogel, J. (2022). An overview of gene regulation in bacteria by small RNAs derived from mRNA 3' ends. *FEMS Microbiol. Rev.* 46, fuac017. <https://doi.org/10.1093/femsre/fuac017>.
 44. Hoyos, M., Huber, M., Förstner, K.U., and Papenfort, K. (2020). Gene autoregulation by 3' UTR-derived bacterial small RNAs. *eLife* 9, e58836. <https://doi.org/10.7554/eLife.58836>.
 45. Esteban-Serna, S., McCaughey, H., and Granneman, S. (2023). Advantages and limitations of UV cross-linking analysis of protein-RNA interactomes in microbes. *Mol. Microbiol.* 120, 477–489. <https://doi.org/10.1111/mmi.15073>.
 46. Melamed, S. (2020). New sequencing methodologies reveal interplay between multiple RNA-binding proteins and their RNAs. *Curr. Genet.* 66, 713–717. <https://doi.org/10.1007/s00294-020-01066-y>.
 47. Melamed, S., Peer, A., Faigenbaum-Romm, R., Gatt, Y.E., Reiss, N., Bar, A., Altuvia, Y., Argaman, L., and Margalit, H. (2016). Global Mapping of Small RNA-Target Interactions in Bacteria. *Mol. Cell* 63, 884–897. <https://doi.org/10.1016/j.molcel.2016.07.026>.
 48. Updegrove, T.B., Shabalina, S.A., and Storz, G. (2015). How do base-pairing small RNAs evolve? *FEMS Microbiol. Rev.* 39, 379–391. <https://doi.org/10.1093/femsre/fuv014>.
 49. Tabib-Salazar, A., Liu, B., Barker, D., Burchell, L., Qimron, U., Matthews, S.J., and Wigneshweraraj, S. (2018). T7 phage factor required for managing RpoS in *Escherichia coli*. *Proc. Natl. Acad. Sci. USA* 115, E5353–E5362. <https://doi.org/10.1073/pnas.1800429115>.
 50. Zahid, M.S., Waise, T.M., Kamruzzaman, M., Ghosh, A.N., Nair, G.B., Mekalanos, J.J., and Faruque, S.M. (2010). The cyclic AMP (cAMP)-cAMP receptor protein signaling system mediates resistance of *Vibrio cholerae* O1 strains to multiple environmental bacteriophages. *Appl. Environ. Microbiol.* 76, 4233–4240. <https://doi.org/10.1128/AEM.00008-10>.
 51. Zhang, S., Zhao, B., Li, J., Song, X., Tong, Y., and An, W. (2022). Host Cyanobacteria Killing by Novel Lytic Cyanophage YongM: A Protein Profiling Analysis. *Microorganisms* 10, 257. <https://doi.org/10.3390/microorganisms10020257>.
 52. Pfeiffer, V., Papenfort, K., Lucchini, S., Hinton, J.C., and Vogel, J. (2009). Coding sequence targeting by MicC RNA reveals bacterial mRNA silencing downstream of translational initiation. *Nat. Struct. Mol. Biol.* 16, 840–846. <https://doi.org/10.1038/nsmb.1631>.
 53. Barquist, L., Westermann, A.J., and Vogel, J. (2016). Molecular phenotyping of infection-associated small non-coding RNAs. *Philos. Trans. R. Soc. Lond. B Biol. Sci.* 371, 20160081. <https://doi.org/10.1098/rstb.2016.0081>.
 54. Ofir, G., and Sorek, R. (2018). Contemporary Phage Biology: From Classic Models to New Insights. *Cell* 172, 1260–1270. <https://doi.org/10.1016/j.cell.2017.10.045>.
 55. Hille, F., Richter, H., Wong, S.P., Bratović, M., Ressel, S., and Charpentier, E. (2018). The Biology of CRISPR-Cas: Backward and Forward. *Cell* 172, 1239–1259. <https://doi.org/10.1016/j.cell.2017.11.032>.
 56. Dunham, D.T., Angermeyer, A., and Seed, K.D. (2023). The RNA-RNA interactome between a phage and its satellite virus reveals a small RNA that differentially regulates gene expression across both genomes. *Mol. Microbiol.* 119, 515–533. <https://doi.org/10.1111/mmi.15046>.
 57. Tabib-Salazar, A., and Wigneshweraraj, S. (2022). RNA Management During T7 Infection. *Phage (New Rochelle)* 3, 136–140. <https://doi.org/10.1089/phage.2022.0029>.
 58. Tree, J.J., Granneman, S., McAtee, S.P., Tolliver, D., and Gally, D.L. (2014). Identification of bacteriophage-encoded anti-sRNAs in pathogenic *Escherichia coli*. *Mol. Cell* 55, 199–213. <https://doi.org/10.1016/j.molcel.2014.05.006>.
 59. Ragunathan, P.T., Ng Kwan Lim, E., Ma, X., Massé, E., and Vanderpool, C.K. (2023). Mechanisms of Regulation of Cryptic Prophage-Encoded Gene Products in *Escherichia coli*. *J. Bacteriol.* 205, e0012923. <https://doi.org/10.1128/jb.00129-23>.

60. Hershko-Shalev, T., Odenheimer-Bergman, A., Elgrably-Weiss, M., Ben-Zvi, T., Govindarajan, S., Seri, H., Papenfort, K., Vogel, J., and Altuvia, S. (2016). Gifsy-1 prophage IsrK with dual function as small and messenger RNA modulates vital bacterial machineries. *PLoS Genet.* 12, e1005975. <https://doi.org/10.1371/journal.pgen.1005975>.
61. Duddy, O.P., Silpe, J.E., Fei, C., and Bassler, B.L. (2023). Natural silencing of quorum-sensing activity protects *Vibrio parahaemolyticus* from lysis by an autoinducer-detecting phage. *PLoS Genet.* 19, e1010809. <https://doi.org/10.1371/journal.pgen.1010809>.
62. Pfeifer, E., Bonnin, R.A., and Rocha, E.P.C. (2022). Phage-Plasmids Spread Antibiotic Resistance Genes through Infection and Lysogenic Conversion. *mBio* 13, e0185122. <https://doi.org/10.1128/mbio.01851-22>.
63. Bandyra, K.J., Bouvier, M., Carpousis, A.J., and Luisi, B.F. (2013). The social fabric of the RNA degradosome. *Biochim. Biophys. Acta* 1829, 514–522. <https://doi.org/10.1016/j.bbagr.2013.02.011>.
64. Skalsky, R.L., and Cullen, B.R. (2010). Viruses, microRNAs, and host interactions. *Annu. Rev. Microbiol.* 64, 123–141. <https://doi.org/10.1146/annurev.micro.112408.134243>.
65. Gouzouasis, V., Tastsoglou, S., Giannakakis, A., and Hatzigeorgiou, A.G. (2023). Virus-Derived Small RNAs and microRNAs in Health and Disease. *Annu. Rev. Biomed. Data Sci.* 6, 275–298. <https://doi.org/10.1146/annurev-biodatasci-122220-111429>.
66. Wang, M., Gu, B., Chen, X., Wang, Y., Li, P., and Wang, K. (2019). The Function and Therapeutic Potential of Epstein-Barr Virus-Encoded MicroRNAs in Cancer. *Mol. Ther. Nucleic Acids* 17, 657–668. <https://doi.org/10.1016/j.omtn.2019.07.002>.
67. Girardi, E., López, P., and Pfeffer, S. (2018). On the Importance of Host MicroRNAs During Viral Infection. *Front. Genet.* 9, 439. <https://doi.org/10.3389/fgene.2018.00439>.
68. Doron, S., Melamed, S., Ofir, G., Leavitt, A., Lopatina, A., Keren, M., Amitai, G., and Sorek, R. (2018). Systematic discovery of antiphage defense systems in the microbial pangenome. *Science* 359, eaar4120. <https://doi.org/10.1126/science.aar4120>.
69. Gottesman, S. (2019). Trouble is coming: Signaling pathways that regulate general stress responses in bacteria. *J. Biol. Chem.* 294, 11685–11700. <https://doi.org/10.1074/jbc.REV119.005593>.
70. Gopalkrishnan, S., Ross, W., Akbari, M.S., Li, X., Hayocks, J.R.J., Grainger, D.C., Court, D.L., and Gourse, R.L. (2022). Homologs of the *Escherichia coli* F Element Protein TraR, Including Phage Lambda Orf73, Directly Reprogram Host Transcription. *mBio* 13, e0095222. <https://doi.org/10.1128/mbio.00952-22>.
71. Skorupski, K., and Taylor, R.K. (1996). Positive selection vectors for allelic exchange. *Gene* 169, 47–52. [https://doi.org/10.1016/0378-1119\(95\)00793-8](https://doi.org/10.1016/0378-1119(95)00793-8).
72. Peschek, N., Herzog, R., Singh, P.K., Sprenger, M., Meyer, F., Fröhlich, K.S., Schröger, L., Bramkamp, M., Drescher, K., and Papenfort, K. (2020). RNA-mediated control of cell shape modulates antibiotic resistance in *Vibrio cholerae*. *Nat. Commun.* 11, 6067. <https://doi.org/10.1038/s41467-020-19890-8>.
73. Datsenko, K.A., and Wanner, B.L. (2000). One-step inactivation of chromosomal genes in *Escherichia coli* K-12 using PCR products. *Proc. Natl. Acad. Sci. USA* 97, 6640–6645. <https://doi.org/10.1073/pnas.120163297>.
74. Robinson, M.D., McCarthy, D.J., and Smyth, G.K. (2010). edgeR: a Bioconductor package for differential expression analysis of digital gene expression data. *Bioinformatics* 26, 139–140. <https://doi.org/10.1093/bioinformatics/btp616>.
75. Melamed, S., Faigenbaum-Romm, R., Peer, A., Reiss, N., Shechter, O., Bar, A., Altuvia, Y., Argaman, L., and Margalit, H. (2018). Mapping the small RNA interactome in bacteria using RIL-seq. *Nat. Protoc.* 13, 1–33. <https://doi.org/10.1038/nprot.2017.115>.
76. Culviner, P.H., Guegler, C.K., and Laub, M.T. (2020). A Simple, Cost-Effective, and Robust Method for rRNA Depletion in RNA-Sequencing Studies. *mBio* 11, e00010–20. 10–1128. <https://doi.org/10.1128/mBio.00010-20>.

STAR★METHODS

KEY RESOURCES TABLE

REAGENT or RESOURCE	SOURCE	IDENTIFIER
Antibodies		
Monoclonal ANTI-FLAG M2 antibody	Sigma-Aldrich	Cat#F1804; RRID: AB_262044
<i>E. coli</i> RNA Polymerase alpha monoclonal antibody 4RA2	BioLegend	Cat#663104; RRID: AB_2687386
Goat anti-rabbit IgG, HRP conjugated	Thermo Fisher Scientific	Cat#A16104; RRID: AB_2534776
Goat anti-mouse IgG, HRP conjugated	Thermo Fisher Scientific	Cat#31430; RRID: AB_228307
Bacterial and virus strains		
<i>Escherichia coli</i> strains	Table S2	N/A
<i>Vibrio cholerae</i> strains	Table S2	N/A
Chemicals, peptides, and recombinant proteins		
TURBO DNA-free Kit	Invitrogen	Cat#AM1907
Blotting-nylon membrane, type B, positive	Sigma-Aldrich	Cat#15356
Protein G Sepharose	Sigma-Aldrich	Cat#P6649
Pierce Protein A/G Magnetic Beads	Thermo Fisher Scientific	Cat# 88803
SUPERase In	Thermo Fisher Scientific	Cat#AM2694
T4 Polynucleotide kinase (PNK)	NEB	Cat#M0201L
T4 RNA ligase 1, high conc	NEB	Cat#M0437M
Streptavidin Magnetic Beads	NEB	Cat#S1420S
Recombinant RNase Inhibitor	Takara	Cat#2313B
Proteinase K (for RIL-seq)	Thermo Fisher Scientific	Cat#EO0491
Terminator 5'Phosphate-Dependent Exonuclease	Lucigen/Biozym	Cat#162370
RNA 5' Polyphosphatase	Lucigen/Biozym	Cat#136120
Poly A Polymerase	enzymatics/Biozym	Cat#280500
GlycoBlue™ Coprecipitant	Thermo Fisher Scientific	Cat#AM9516
Superscript III first strand kit	Thermo Fisher Scientific	Cat#18080051
Protease Inhibitor Cocktail Set III, EDTA-Free	Merck - Millipore	Cat#539134-1ML
RNase A/T1 mix	Thermo Fisher Scientific	Cat#EN0551
AMPure XP Beads	Beckman Coulter Life Sciences	Cat#A63881
SPRISelect	Beckman Coulter Life Sciences	Cat#B23317
DNase I (RNase-free)	NEB	Cat#M0303L
Monarch® RNase A	NEB	Cat#T3018L
Proteinase K, Molecular Biology Grade	NEB	Cat#P8107S
NEBNEXT Ultra II Q5 Master Mix	NEB	Cat#M0544S
Gibson Assembly® Master Mix	NEB	Cat#E2611L
Protein G Sepharose, fast flow	Sigma-Aldrich	Cat#P3296
NEBNEXT® Magnesium RNA Fragmentation Module	NEB	Cat#E6150S
Critical commercial assays		
NEBNEXT® Multiplex Small RNA Library Prep Set for Illumina®	NEB	Cat#E7300L
Luna® Universal One-Step RT-qPCR Kit	NEB	Cat#E3005X
Monarch® Plasmid Miniprep Kit	NEB	Cat#T1010L
Monarch® HMW DNA Extraction Kit for Tissue	NEB	Cat#T3060L
RNA Clean & Concentrator™ 5	Zymo Research	Cat#R1013
Monarch® RNA Cleanup Kit (10 µg)	NEB	Cat#T2030L
Agilent RNA 6000 Nano Kit	Agilent	Cat#5067-1511

(Continued on next page)

Continued

REAGENT or RESOURCE	SOURCE	IDENTIFIER
Agilent RNA 6000 Pico Kit	Agilent	Cat#5067-1513
Agilent High Sensitivity DNA Kit	Agilent	Cat#5067-4626
NextSeq 1000/2000 P ² Reagents (100 Cycles) v2	Illumina	Cat#20046811
NextSeq 1000/2000 P ² Reagents (200 Cycles) v2	Illumina	Cat#20046812
Deposited data		
Raw and analyzed Data: RNAseq VP882	This paper	GEO: GSE247770
Raw and analyzed Data: RIPseq	This paper	GEO: GSE247768
Raw and analyzed Data: RILseq	This paper	GEO: GSE247767
Raw and analyzed Data: RNAseq VP882 wild-type vs ΔvpdS	This paper	GEO: GSE247769
Oligonucleotides		
DNA oligonucleotides used in this study	Table S4	N/A
Recombinant DNA		
Plasmids generated in this study	Table S3	N/A
Software and algorithms		
CLC Genomics Workbench	Qiagen	https://qiagenbioinformatics.com RRID:SCR_011853
BaseSpace Sequence hub	Illumina	https://euc1.sh.basespace.illumina.com RRID:SCR_011881
RNAfold	UniVie	http://rna.tbi.univie.ac.at/cgi-bin/RNAWebSuite/RNAfold.cgi RRID:SCR_024427
IntaRNA	Freiburg RNA Tools	http://rna.informatik.uni-freiburg.de/IntaRNA/Input.jsp
Prism 9	GraphPad	https://www.graphpad.com/
RNAhybrid	Universität Bielefeld BibiServ	http://bibiserv2.cebitec.uni-bielefeld.de RRID:SCR_003252
ChimericFragments	Huber et al. ²³	https://github.com/maltesie/ChimericFragments

RESOURCE AVAILABILITY

Lead contact

Further information and requests for resources and reagents should be directed to and will be fulfilled by the lead contact, Kai Papenfort (kai.papenfort@uni-jena.de).

Materials availability

This study did not use or generate any unique reagents.

Data and code availability

- All sequencing data has been deposited at Gene Expression Omnibus (GEO) under the accession codes GSE247770 (RNA-seq and dRNA-seq of VP882), GSE247768 (RIP-seq), GSE247767 (RIL-seq) and GSE247769 (RNAseq of VP882 and VP882 ΔvpdS phage activation) and are publicly available as of the date of publication.
- This paper does not report original code.
- Any additional information required to reanalyze the data reported in this paper and original Northern and Western blot images will be available from the [lead contact](#) upon request.

EXPERIMENTAL MODEL AND SUBJECT DETAILS

Bacterial strains

Throughout the study, *V. cholerae* C6706 was used as the wild-type strain. All strains used in this study is listed in [Table S2](#). *V. cholerae* and *E. coli* strains were grown aerobically in LB broth (Lennox) or M9 medium (0.4 % glucose) at 37 °C and 200 rpm

except for temperature-sensitive strains. Unless otherwise noted, antibiotics were used at the following concentrations: 100 µg mL⁻¹ ampicillin, 50 µg mL⁻¹ kanamycin (in M9 medium: 25 µg mL⁻¹), 20 µg mL⁻¹ chloramphenicol (in M9 medium: 10 µg mL⁻¹), 50 µg mL⁻¹ hygromycin B, 6.25 µg mL⁻¹ polymyxin B; and 5,000 µg mL⁻¹ streptomycin. Synchronization before temperate phage induction was achieved by a 1:10 back-dilution at OD₆₀₀ 0.4 in M9 medium with 0.035% arabinose to induce VqmA_{phage} expression. Phage activation was stimulated with 25 µM DPO. To monitor growth over time, 200 µL culture was dispensed into a 96-well plate in technical triplicates and absorbance at 600 nm was measured at 37 °C every 15 min using the Spark 10M plate reader (Tecan). To calculate relative survival, serial dilutions of bacterial cultures were spotted on agar plates and colony-forming units were determined (wild-type survival set to 100%). For transient inactivation of RNase E, *V. cholerae* wild-type and a temperature-sensitive strain harboring the *rne-3071* mutation (*rne*^{TS}) were grown at 30 °C to the indicated cell density. Cultures were divided in half and either continuously grown at 30 °C or shifted to 44°C for 30 min. RNA samples were collected from both temperatures at indicated time points after the plasmid-borne *gp29-vpdS* induction. Plasmids were introduced into recipient *V. cholerae* cells by RK2/RP4-based conjugal transfer from *E. coli* S17λpir plasmid donor strains. For plasmid transfer from *E. coli* Top10, S17λpir helper strains were used in a triparental mating. VP882 phage was introduced to *V. cholerae* on previously described protocols.⁹ Mixtures of donor, helper and recipient were incubated on LB agar plates at 37°C for at least 4h dependent on the transferable plasmid (pKAS32 and VP882: 16h, other plasmids up to 8h). Trans-conjugants were selected using appropriate antibiotics and polymyxin B to specifically inhibit *E. coli* growth. *V. cholerae* mutant strains were generated as described previously.⁷¹ Briefly, pKAS32 plasmid transfer was selected on agar plates containing ampicillin. Single colonies were streaked on streptomycin plates for counter-selection and tested for desired mutations by PCR or sequencing.

METHOD DETAILS

Plasmid construction

The plasmids used in this study are listed in **Table S3**, DNA oligonucleotides are listed in **Table S4**. For pMS-100, pMH-001 and pMS-257, the cm^R cassette was amplified with KPO-1518/1519 from pEVS143-C and cloned by Gibson assembly into KPO-1520/1521-linearized pCMW-2K, pMD-004 and pKP-361, respectively. pMS-137 was generated by amplification of *gp29-vpdS* from VP882 chromosomal DNA using KPO-8433/8434 and Gibson assembly with pMD004 linearized with KPO-0196/1397. pMS-141 and pMS-142 were generated by amplification of *vpdS* from VP882 chromosomal DNA using KPO-8438/8434 and Gibson assembly with pEVS143-K and pEVS143-C, respectively, linearized with KPO-0092/1397. The M1, M2 and M3 point mutations were introduced into pMS-141 by site-directed mutagenesis with KPO-8626/8627, KPO-8585/8586 and KPO-9087/9088, yielding pMS-156, pMS-155 and pMS-203, respectively. The M1 mutation in pMS-228 was obtained by site-directed mutagenesis of pMS-142 with KPO-8626/8627. pMS-177 was constructed by amplification of full-length *tarB* from KPS-0014 chromosomal DNA using KPO-8773/8774 and Gibson assembly with pEVS143-K linearized with KPO-0092/1397. For pMS-198, the cm^R cassette was amplified with KPO-1518/1519 from pEVS143-C and cloned into pMS-177 linearized with KPO-1520/1521 by Gibson assembly. pMS-189 and pMS-226 were obtained by site-directed mutagenesis of pMS-177 and pMS-198, respectively, with KPO-8939/8940. For the plasmid pMS-260, *hfq* was amplified from KPS-0014 chromosomal DNA using KPO-9809/9810 and cloned by Gibson assembly into KPO-4051/pBAD-ATGrev-linearized pMD373. The cm^R cassette was cloned into pMS-261 by Gibson assembly of KPO-1520/1521-linearized pMS-260 with KPO-1520/1521 and the cm^R cassette, amplified with KPO-1518/1519 from pEVS143-C. For transcriptional reporters, pMS-258 and pMS-259 were generated by amplification of the vcr017 and vcr068 promoter regions from KPS-0014 chromosomal DNA using KPO-9802/9803 and KPO-9807/9808, respectively and Gibson assembly with pMS-257 linearized with KPO-1953/9804. For translational GFP reporter fusions, the pXG10 and pXG30 vectors were used for monocistronic genes and operons, respectively. Bacterial and viral target inserts were amplified from KPS-0014 chromosomal DNA and VP882 genomic DNA, respectively, using the corresponding oligonucleotide combinations indicated in the following and cloned into pXG10 linearized with KPO-1702/1703 via Gibson assembly: pMS-148 (*petA*, KPO-8566/8567), pMS-149 (*frhC*, KPO-8568/8569), pMS-151 (*gp02*, KPO-8572/8573), pMS-164 (*vexA*, KPO-8701/8702), pMS-166 (*vca0808*, KPO-8707/8708), pMS-232 (*glyA*, KPO-9274/9275), pMS-195 (*gp69*, KPO-8916/8722). For pKP-464 (KPO-1062/1063) and pKP-479 (KPO-1046/1047), pXG10 and respective inserts were digested with *Nsi*I and *Nhe*I and ligated. Of note, the DNA insert length for each reporter was based on the RNA duplex predictions presented in **Figures S3B–S3L**. To remove the terminator structure in the 5'UTR of *gp69*,⁹ pMS-195 was amplified by KPO-9058/9059 yielding in pMS-202. For pMS-234 and pMS-237, *hemH* (KPO-9278/9279) and *gp38* (KPO-9343/9344) were amplified, respectively, and cloned into pXG30 linearized with KPO-4646/1703 via Gibson assembly. Point mutations in the translational reporters of *rpoS* (pKP-479), *gp02* (pMS-151), *cyaA* (pJR-26) and *petA* (pMS-148) were implemented by PCR using KPO-9199/9200, KPO-9341/9342, KPO-8589/8590 and KPO-9093/9094 resulting in pMS-220, pMS-235, pMS-154 and pMS-201, respectively. The plasmids pMS-186, pKAS32-*rpoS*::3XFLAG and pMS-160 were constructed by Gibson assembly using pKAS32 linearized with KPO-0267/0268. The insert fragments were amplified from KPS-0014 chromosomal DNA for pMS-186: KPO-8827/8828 and KPO-8829/8830, for pKAS32-*rpoS*::3XFLAG: KPO-1566/1567 and KPO-1568/1569 and for pMS-160: KPO-6033/6034 and KPO-6037/6038. The FLAG sequence of pMS-160 was amplified from KPS-0995 using KPO-6035/6036.

RNA isolation, Northern blot analysis and quantitative real-time PCR

Culture aliquots (4 OD₆₀₀ units) were collected at indicated time points or cell densities and mixed with 0.2 vol of stop solution (95% ethanol, 5% phenol). Total RNA was extracted using the Extrazol reagent (blirt) and blotted as described previously.²⁶ Nylon

membranes (Sigma) were hybridized in ROTI®Hybri-Quick with [³²P] end-labeled DNA oligonucleotides at 42 °C. Membranes were washed in three subsequent steps with SSC (5x, 1x, 0.5x)/0.1% SDS wash buffer. Signals were visualized using a Typhoon Phosphorimager (GE Healthcare). Oligonucleotides for Northern Blot analyses are provided in [Table S4](#). In case of probing for several target sRNAs, membranes were stripped with 30 mL ROTI®Hybri-Quick at 72°C for at least 2h. For qRT-PCR, 20 µg total RNA were digested with TurboDNase at 37°C for 30 min and precipitated overnight in 75% ethanol and 75 mM sodium acetate pH 5.5. qRT-PCR was performed using the Luna Universal One-Step RT-qPCR Kit (New England BioLabs) and CFX96 Real-Time PCR System (Bio-Rad). 5S rRNA and recA were used as reference genes. Oligonucleotides used for qRT-PCR are provided in [Table S4](#).

Western blot analysis and fluorescence assays

Total protein sample preparation and Western blot analyses were performed as described previously.²⁴ Signals were visualized using a Fusion FX EDGE imager (Vilber) and band intensities were quantified using the GelQuant software (biochemlabsolutions). Chromosomally 3XFLAG-tagged Hfq, CyaA and RpoS were detected using anti-FLAG antibody (Sigma). RnaP α served as a loading control and was detected using anti-RNAp α antibody (BioLegend). Fluorescence measurements of *V. cholerae* and *E. coli* Top10 cells expressing transcriptional GFP reporter or translational GFP fusion were performed as described previously.⁷² For transcriptional reporter assays in *V. cholerae*, cells were grown in M9 medium to the desired time point. *E. coli* cells were grown overnight in LB medium and the respective antibiotics. All cells were washed with and resuspended in PBS. The relative fluorescence intensity was determined using the Spark 10M plate reader (Tecan). Non-fluorescent cells were used as autofluorescence controls.

Generation of phage mutant strains

The $\Delta vpdS::FRT$ VP882 phage was generated by PCR amplification of the FRT-cm^R-FRT cassette of pKD-3 using KPO-8630/8131 and KPO-8631/8132 followed by lambda red recombination.⁷³ Both PCR products were joined by overlap PCR using KPO-8632/8633 and purified using gel extraction. The deletion cassette was transformed into electrocompetent Top10 cells co-transformed with the phage JSP-1269 and pKD-46 to replace the phage gene *vpdS* by homologous recombination. Positive clones were selected on LB agar containing kanamycin and chloramphenicol and verified by colony-PCR. The loss of pKD-46 was achieved by overnight incubation at 37°C. To remove the chloramphenicol resistance cassette from the phage DNA, positive clones were co-transformed with pFLP-hyg (constitutive expression of FLP) and selected on LB agar containing kanamycin and hygromycin at 30°C. The loss of the pFLP-hyg plasmid was achieved by growth at 44°C overnight in liquid medium and the excision of the chloramphenicol cassette was verified by PCR and selective growth on LB agar containing kanamycin, kanamycin and chloramphenicol or kanamycin and hygromycin.

Phage DNA preparation and quantitative PCR

Synchronized cultures of *V. cholerae* lysogenized with VP882 were grown to OD_{600nm} 0.2 and 50 mL were harvested (0 min sample). The cultures were stimulated with 25 µM DPO and returned to growth. After 30, 60 and 120 min post induction, 50 mL culture aliquots were taken and cleared from unlysed cells and debris by centrifugation at 4,700 rpm and 4°C for 10 min followed by filtration through 0.2 µm filter. The filtrate was incubated with 100 U DNase I (NEB) and 1 mg Monarch RNase A (NEB) at 37°C for 30 min to digest host nucleic acids. Phage particles were precipitated by addition of 16.7 mL 5 M NaCl and 16.7 mL 50% PEG-8000 overnight at 4°C. Viral particles were collected by centrifugation (20,000 x g, 4°C and 20 min) and the phage pellet was soaked in 300 µL 5 mM MgSO₄ for at least 30 min on ice. The phage DNA was isolated using the Monarch® HMW DNA Extraction Kit for Tissue according to the manufacturer's protocol for phage DNA isolation. Each sample was spiked with 500 ng pUC19 plasmid DNA for relative quantifications. Briefly, the phages were digested with Proteinase K and the released DNA was precipitated with isopropanol on the surface of large glass beads. After two washing steps, the DNA was recovered in 50 µL elution buffer. For quantitative PCR (qPCR) 1 µL DNA was used with the GoTaq qPCR Master Mix (Promega, #A6002) and the CFX96 Real-Time PCR System (Bio-Rad). The *ampR* gene in pUC19 was used as reference gene. Oligonucleotides used for qPCR are listed in [Table S4](#).

RNAseq and dRNAseq VP882 activation

V. cholerae Δtdh strain lysogenized with VP882 (JSP-1269) was cultivated in triplicates in M9 medium. Synchronized cultures at OD₆₀₀ 0.2 were treated with 25 µM DPO and at indicated time points, transcription was stopped by adding 0.2 volumes of stop mix (95% ethanol, 5% [vol/vol] phenol). Total RNA was isolated, treated with Turbo DNase (Thermo Fisher Scientific) and the RNA integrity was confirmed using a Bioanalyzer (Agilent). cDNA libraries were prepared by vertis Biotechnology AG in a 3' end-specific protocol. The rRNA depleted RNAs samples were fragmented using ultrasound (4 pulses of 30 sec at 4°C). An oligonucleotide adapter was ligated to the 3' OH end of the RNA molecules. First-strand cDNA synthesis was performed using M-MLV reverse transcriptase and the 3' adapter as primer. The first-strand cDNA was purified, and the 5' Illumina TruSeq sequencing adapter was ligated to the 3' end of the antisense cDNA. Finally, 3' cDNA fragments were amplified, purified using the Agencourt AMPure XP kit (Beckman Coulter Genomics). For the dRNA-seq approach, RNA samples from the same replicate at different time points were pooled in equal amounts (2.5 µg each). The pooled RNA samples were fragmented using ultrasound (4 pulses of 30 sec at 4°C) followed by T4 Polynucleotide Kinase (NEB) treatment. The samples were split into two halves and one half was subjected to Terminator Exonuclease treatment (+TEX; Lucigen), the other half was left untreated (-TEX). The RNA samples were

poly(A)-tailed using poly(A) polymerase and the 5'PPP structures were removed using RNA 5' Polyphosphatase (Lucigen). The RNA adapter was ligated to the 5'- monophosphate of the RNA and first-strand cDNA synthesis was performed using an oligo(dT)-adapter primer and the M-MLV reverse transcriptase. cDNA fragments were PCR-amplified and purified using the Agencourt AMPure XP kit (Beckman Coulter Genomics). All cDNA libraries were sequenced using a NextSeq1000 system with 100-nt read length in single-read mode. Demultiplexed raw reads were trimmed for quality and 3' adaptors and mapped to the *V. cholerae* and VP882 reference genomes (NCBI accession numbers NC_002505.1, NC_002506.1, NC_009016.1) using "RNA-Seq Analysis" tool of CLC Genomics Workbench (Qiagen) with standard parameter settings. The CLC Genomics Workbench was further used to count the reads mapped to the annotated genes, and to calculate differential gene expression. The CLC Genomics Workbench utilizes TMM normalization and compares gene expression between conditions using the edgeR algorithm.⁷⁴ Genes with a fold change $\geq \pm 1.5$ and an FDR-adjusted *p*-value ≤ 0.05 were defined as differentially expressed. For transcription start site (TSS) annotation in the VP882 phage the coverage in plus and minus TEX conditions and based on it the difference between neighboring nucleotides was computed. Local maxima in the differences were called as TSS and the set of putative TSS was then curated by hand.

Hfq coimmunoprecipitation and RIP-seq analysis

V. cholerae Δtdh and $\Delta tdh\ hfq::3XFLAG$ strains lysogenized with VP882 (JSP-1269) were cultivated in triplicates in M9 medium. Synchronized cultures at OD₆₀₀ 0.2 were divided, treated either with 25 μ M DPO or water and incubated for 60 min at 37°C and 200 rpm. Cells equivalent to 50 OD₆₀₀ units were subjected to immunoprecipitation as previously described.²³ Briefly, Hfq-bound RNA was enriched using monoclonal anti-FLAG antibody (Sigma, #F1804) and Protein G Sepharose (Sigma, #P3296). After five stringent washing steps with lysis buffer, RNA and protein fractions were separated by phenol-chloroform-isopropanol extraction. The RNA was treated with DNase I (Thermo Fisher Scientific), and RNA integrity was tested on an Agilent 2100 Bioanalyzer. cDNA libraries were prepared using the NEBNext Small RNA Library Prep Set for Illumina (NEB; E7300L) according to the manufacturer's instructions. cDNA library quality was confirmed on an Agilent 2100 Bioanalyzer and pooled cDNA libraries were sequenced on a NextSeq1000 system with 100-nt read length in single-read mode. Demultiplexed raw reads were trimmed for quality and adaptors and mapped to the *V. cholerae* and VP882 reference genome (NCBI accession numbers NC_002505.1, NC_002506.1, NC_009016.1) using CLC Genomics Workbench (Qiagen) with standard parameter settings as described above. Fold enrichment in the *hfq::3XFLAG*-tagged samples was compared to the untagged control samples (Δtdh) using the CLC "Differential Expression for RNA-Seq" tool. Read counts (TPM values) matching to a given category (phage transcript, host sRNA, host tRNA and host rRNA) were compared to the total number of TPM in the same cDNA library.

Hfq RIL-seq and computational analysis

Samples were collected like in the RIP-seq approach and processed following the original RIL-seq protocol.⁷⁵ Briefly, cells corresponding to 50 OD₆₀₀ units were subjected to protein and RNA UV-crosslinking followed by cell lysis and co-immunoprecipitation using a monoclonal anti-FLAG antibody (Sigma; F1804). Recovered RNA was trimmed by RNase A/T1 treatment, and proximal RNAs were ligated using T4 RNA ligase. After protein digestion using proteinase K, RNA was extracted, fragmented and TurboDNase digested. Ribosomal RNA was depleted using rRNA-specific biotinylated probes.⁷⁶ Co-immunoprecipitated RNA was mixed with 1X SSC, 1 mM EDTA and an oligonucleotide mix (5.8 nM for 16S and 23S oligos; 11.6 nM for 5S oligos). The mixture was denatured, cooled down and incubated with streptavidin beads (ThermoFisher; 65001) at room temperature and 50°C, each step 5 min, respectively. rRNA depleted RNA was purified using the Agencourt AMPure XP kit (Beckman Coulter Genomics) and subjected to cDNA library preparation. The NEBNext Ultra II Q5 polymerase was used for library amplification. DNA libraries were sequenced on a NextSeq1000 system with 200-nt read length in paired-end mode. The computational analysis was adapted from the following protocol.²³ Demultiplexed raw sequencing reads were checked for quality and regions of low-quality tails and complexity were removed. The remaining reads were mapped to the *V. cholerae* and VP882 reference genome (NCBI accession numbers NC_002505.1, NC_002506.1, NC_009016.1). The alignments were referred to the annotations of the host (sRNA, CDC_UTRs, intergenic region) and VP882 (phage transcript) reference genome, including the annotation of the newly identified sRNA VpdS. The interactions (chimeric reads) were then filtered by their number and their statistical significance using a cut-off of 5 reads per interaction and an FDR-adjusted *p*-value ≤ 0.05 .

RNA-seq analysis of VP882 wild-type and VP882 $\Delta vpdS$

V. cholerae Δtdh strain lysogenized with VP882 wild-type and VP882 $\Delta vpdS$ were cultivated in triplicates in M9 medium. Synchronized cultures at OD₆₀₀ 0.2 were treated with 25 μ M DPO and at indicated time points, transcription was stopped by adding 0.2 volumes of stop mix (95% ethanol, 5% [vol/vol] phenol). Total RNA was isolated, treated with Turbo DNase (Thermo Fisher Scientific) and the RNA integrity was confirmed using a Bioanalyzer (Agilent). Ribosomal RNA was depleted using rRNA-specific biotinylated probes⁷⁶ as described above. rRNA depleted RNA was purified using the Agencourt AMPure XP kit (Beckman Coulter Genomics) and fragmented for 5 min at 75°C using the NEBNext® Magnesium RNA Fragmentation Module (NEB). cDNA libraries were prepared using the NEBNext Small RNA Library Prep Set for Illumina (NEB; E7300L) according to the manufacturer's instructions. cDNA library quality was confirmed on an Agilent 2100 Bioanalyzer and pooled cDNA libraries were sequenced on a NextSeq1000 system with 100-nt read length in single-read mode. Demultiplexed raw reads were trimmed for quality and adaptors and mapped to the *V. cholerae* and VP882 reference genome (NCBI accession numbers NC_002505.1, NC_002506.1, NC_009016.1) using the

“RNA-Seq Analysis” tool of the CLC Genomics Workbench (Qiagen) with standard parameter settings as described above. Genes with a fold change $\geq \pm 1.3$ and an *p*-value ≤ 0.05 were defined as differentially expressed.

QUANTIFICATION AND STATISTICAL ANALYSIS

Statistical analysis was performed using Graph Pad Prism 9 (GraphPad Software Inc.). Data are presented as the mean \pm SD. The number of technical and independent biological replicates for each experiment is indicated in the figure legends or methods. No blinding or randomization was used in these experiments. Statistical details of experiments can be found in figure legends. Statistical analysis of the RIL-seq experiment was performed as previously described.²³ Band intensities of blot images was quantified with GelQuantNet (biochemlabsolutions) and analyzed with Graph Pad Prism 9.